DETERMINATION OF NEUTRON-INDUCED ACTIVATION CROSS SECTIONS USING NIRR-1

AHMADU BELLO UNIVERSITY, ZARIA.

BY

SADIQ Umar

Ph.D/SCI/31309/2001-02

A DISSERTATION
SUBMITTED TO THE POST GRADUATE SCHOOL,
AHMADU BELLO UNIVERSITY, ZARIA
IN PARTIAL FULFILLMENT OF THE REQUIREMENTS
FOR THE AWARD OF
DOCTOR OF PHILOSOPHY DEGREE (PhD) IN PHYSICS.

FACULTY OF SCIENCE

DEPARTMENT OF PHYSICS

DEPARTMENT OF PHYSICS,
AHMADU BELLO UNIVERSITY, ZARIA
JUNE, 2007

JUNE, 2006

DEDICATION

I dedicate this work to my mother, wife and children.

DECLARATION

This dissertation titled

"Determination of Neutron-Induced Activation Cross Sections Using NIRR-1" is the outcome of my research work under the supervision of Prof. S. A. Jonah. To the best of my knowledge, no part thereof has been submitted to any other institution for the award of a degree other than Ahmadu Bello University, Zaria. All references cited are duly acknowledged.

_____

SADIQ, Umar

CERTIFICATION

This dissertation titled "Determination of Neutron-Induced Activation Cross Sections Using NIRR-1" meets the regulations governing the award of the degree of Doctor of Philosophy in Physics of Ahmadu Bello University, and is approved for its contribution to knowledge and literary presentation.

_____	_____
Prof. S. A. Jonah	Date
Chairman, Supervisory Committee.	
_____	_____
Prof. N. Hariharan	Date
Member, Supervisory Committee.	
_____	_____
Prof. N. Hariharan	Date
Head, Department of Physics.	
_____	_____
Dean, Postgraduate School.	Date

ACKNOWLEDGEMENT

I wish to express my indebtedness and sincere gratitude to Prof. S. A. Jonah for his patience, guidance and understanding throughout the course of this work -Thank you. I also wish to express my appreciation to Prof. N. Hariharan for his suggestions and encouragement and to Mrs. Hariharan for her prayers.

I would like to thank Mr. S. A. Osasona for his concern, support and prayers, and my other colleagues in the Department of physics, A.B.U. Zaria, for the roles they played variously in the course of this work. I thank you all.

ABSTRACT

The full-energy peak efficiency (FEP) curves of the gamma-ray spectrometry setup for use with the newly commissioned Nigeria Research Reactor-1 (NIRR-1) have been determined at three source-detector positions aimed at routine neutron activation analysis with the reactor. Standard gamma ray sources were used to determine the efficiency curves in the energy range of 59.5-2240.1 keV and a semi-empirical approach was used to extend the efficiency data from 2204.1 keV to 4000 keV. The semi-empirical method has been found to be reasonably accurate within experimental uncertainties.

The neutron spectrum parameters (i.e. the thermal-to-epithermal flux ratio, f, and the epithermal flux shape factor, α) for one inner and one outer (A1 and A2) irradiation channels of NIRR-1, required (or needed) for the extension of its applicability to k_0-NAA, were determined using the "Cd-ratio for multi-monitor method". For the general applicability of the k_0-NAA to deal with "non-1/v" (n, γ) reactions, the modified spectral index, $r(\alpha)\sqrt{(T_n/T_0)}$, and Westcott's $g(T_n)$ factor for monitoring neutron temperature T_n were also determined for the two irradiation channels. Neutron spectrum parameters determined in the inner channel A1, are: $\alpha = -0.046 \pm 0.005$; $f = 18.4 \pm 0.34$; $r(\alpha)\sqrt{(T_n/T_0)} = 0.04878$; $T_n = 38.81^0$(Holden) and $g(T_n) = 11.30, 1.883$. For the outer channel A2, the values are: $\alpha = +0.024 \pm 0.002$;

$f = 49.5 \pm 0.96$; $r(\alpha)\sqrt{(T_n/T_0)} = 0.01786$; $T_n = 30.22^0$(Holden) and $g(T_n) = 13.89, 1.821$.

The results are in good agreement with reported values from other reactor facilities with similar core configuration.

The thermal radiative capture cross sections, σ_0 and k_0-factors for ten (n,γ) reactions i.e. ^{197}Au (n, γ) ^{198}Au; ^{94}Zr (n, γ) ^{95}Zr ; ^{96}Zr (n, γ) ^{97}Zr ; ^{238}U (n, γ) ^{239}U ; ^{55}Mn (n, γ) ^{56}Mn ;

^{109}Ag (n, γ) ^{110m}Ag ; ^{48}Ca (n, γ) ^{49}Ca ; ^{71}Ga (n, γ) ^{72}Ga ; ^{74}Se (n, γ) ^{75}Se and ^{75}As (n, γ) ^{76}As have been reevaluated and the results compare well with evaluated data from libraries and Mughabghab, (2003). This work has been undertaken as part of an IAEA Coordinated Research Project No.13728 entitled “Reference Database for NAA”.

TABLE OF CONTENTS

Title page		i
Declaration		ii
Certification		iii
Dedication		iv
Acknowledgements		v
Abstract		vi
Table of contents		viii
List of tables		xi
List of figures		xii
CHAPTER ONE: INTRODUCTION		
1.1	General introduction	1
1.2	Review of previous works	5
1.3	Present work	6
1.4	Outline of work	7
CHAPTER TWO: THEORETICAL FRAMEWORK		
2.0	Neutrons	8
2.1.0	Neutron Interaction with matter	10
2.1.1	Absorption	10
2.1.2	Scattering	11
2.1.3	Neutron reaction cross sections	12
2.2	Interaction of radiation with matter	14

2.2.1	Charged particle radiation	14
2.2.1.1	Electrons	14
2.2.1.2	Positrons	16
2.2.1.3	Heavy charged particles	16
2.2.2	Uncharged particle radiation	17
2.2.2.1	Electromagnetic radiation	17
2.2.2.1.1	Photoelectric effect	17
2.2.2.1.2	Compton effect	18
2.2.2.1.3	Pair production	19
2.3	Theory of activation analysis	19
2.3.1	The Høgdahl's convention	28
2.3.2	Neutron self shielding and Cd-transmission factors	29
2.3.3	The activation equation	30
2.3.4	Principles of standardization	32
2.3.5	Relative standardization	33
2.3.6	The absolute method	35
2.3.7	The single comparator method	35
2.3.8	The k_0-standardization	36
2.4	Determination of f and α-values	40
2.5	Monitoring specific flux parameters	42

CHAPTER THREE: MATERIALS AND METHODS

3.1 Materials 45

3.1.1 Standard sources 45

3.1.2 Monitor foils 46

3.1.3 Reaction cross sections determination 46

3.1.4 The NIRR-1 49

3.1.5 Gamma-ray spectrometer 51

3.2 Methodology 51

3.2.1 Efficiency calibration of the HPGe 51

3.2.2 Site characterization 54

3.2.3 Cross section and $k_{0,Au}$ determination 62

CHAPTER FOUR: RESULTS AND DISCUSSION

4.1 Calibration 64

4.2 Cadmium ratios 71

4.3 f and α 72

4.4 Neutron flux 76

4.5 Westcott's g-factor, Modified Spectral Index and Neutron temperature. 76

4.6 Cross-sections 78

CHAPTER FIVE: CONCLUSION AND RECOMMENDATIONS

5.0 Conclusion 84

5.1 Recommendations 85

References 86

LIST OF TABLES

page

Table 3.1	Nuclear data of standard gamma sources	45
Table 3.2	Description of the monitor foils used.	46
Table 3.3a	Description of monitor foils and oxides used.	47
Table 3.3b	Nuclear data of monitor foils and oxides used.	48
Table 3.4	Physical constants of Al and Ge used in the efficiency calculations	53
Table 3.5	Nuclear data for the nuclides used as monitors	56
Table 3.6a	Irradiation, decay and counting regimes for irradiation site A1.	56
Table 3.6b	Irradiation, decay and counting regimes for irradiation site A2	57
Table 3.7	$k_{0,Au}$ factors and related nuclear data .	61
Table 3.8	$g_{Lu}(T_n)$ versus T_n	62
Table 4.7	Calculated values of R_{Cd} for NIRR-1 and nuclear data of detector monitors.	71
Table 4.8	Comparison of f and α values in irradiation channels of Slowpoke and MNSR facilities	73
Table 4.9	Neutron fluxes.	76
Table 4.10	Westcott's g-factor, Modified Spectral Index and Neutron Temperature.	77
Table 4.11	Comparison of Calculated Activation cross section σ_0 and libraries.	80
Table 4.12	Calculated k_0-factors and other parameters	82

LIST OF FIGURES

page

Fig. 2.1 A typical reactor neutron energy spectrum showing the various components used to describe the neutron energy regions 8

Fig 2.2 Diagram illustrating the process of neutron capture by a target nucleus followed by the emission of gamma rays. 10

Fig. 2.3a Representation of the (n, γ) cross-section function σ(E) versus E 23

Fig. 2.3b. Representation of the reactor neutron flux distribution φ'(E) versus E 23

Fig. 2.4a Cd total cross section curve, $\sigma_{tot,Cd}(E)$ versus E 24

Fig. 2.4b. Actual and idealized Cd neutron transmission functions, T(E) and t(E) versus E 24

Fig 3.1 NIRR-1 Core configuration showing the irradiation channels 50

Fig.4.1a ln Eff. vs ln E at 1cm source-detector distance 65

Fig.4.1b ln Eff. vs ln E at 5cm source-detector distance 66

Fig.4.1c ln Eff. vs ln E at 15cm source-detector distance 67

Fig.4.2a Efficiency curves of a HPGe detector vs gamma energy at 1cm. 68

Fig.4.2b Efficiency curves of a HPGe detector vs gamma energy at 5cm 69

Fig.4.2c Efficiency curves of a HPGe detector vs gamma energy at 15cm 70

Fig.4.3 Determination of *f* and α by "Cd Ratio for multi monitor" method for inner irradiation Channel A1, of NIRR-1 74

Fig.4.4 Determination of *f* and *α* by "Cd Ratio for multi monitor" method for outer irradiation Channel A2, of NIRR-1 75

Fig.4.5 Comparison of Mughabghab with our result and other evaluated data 81

Fig.4.5 Comparison of k_0-factors for Mughabghab with our result 83

CHAPTER ONE
INTRODUCTION

1.1 General introduction

Neutron activation analysis (NAA) was discovered in 1936 when Hevesy and Levi found that samples containing certain rare earth elements became highly radioactive after exposure to a source of neutrons (Glascock, 1996). From this observation, they quickly recognized the potential of employing nuclear reactions on samples followed by measurement of the induced radioactivity to facilitate both qualitative and quantitative identification of the elements present in the samples.

Neutron activation analysis (NAA) is a sensitive analytical technique useful for performing both quantitative and qualitative multi-element analysis of major, minor and trace elements in samples from almost every conceivable field of scientific and or technical interest. It is based on the measurement of characteristic gamma rays emitted by isotopes of the sample that are produced by irradiation with thermal, epithermal or fast neutrons. Typically, the sample and the standard, for the elements of interest, are irradiated for a fixed period of time in the neutron flux from a neutron source. After the irradiation and appropriate radioactive decay (cooling time), the gamma energy spectrum is measured by counting the sample on a high resolution detection system (HPGe detector), where the gamma ray detected at a particular energy are indicative of a specific radionuclide present.

In gamma-ray spectroscopy there is the need to establish the energy dependent full-energy peak (FEP) efficiency because, absolute gamma-ray emission rates and quantitative analyses can be obtained only with detectors that have been calibrated for FEP efficiency, also the full-energy peak detection efficiency, $\varepsilon_{p,}$ has to be introduced in the relevant

equations for experimental k_0-measurement for the determination of concentration of the analyte and also for the determination of thermal-to-epithermal flux ratio, *f*, and the epithermal flux shape factor, α. (De Corte, 1987). The efficiency is a measure of the probability that a gamma ray, of a given energy, is fully absorbed in the active volume of a detector. Since the gamma-ray detection is the key to obtaining good quality results, the detector calibration is essential for high precision analysis and reliance on experimentally measured values of the k_0-factors.

The sensitivities for NAA are dependent upon the irradiation parameters, (i.e. irradiation time, neutron flux and decay time) measurement conditions (i.e. measurement time, detector efficiency) and nuclear parameters of the element being measured (i.e. isotopic abundance, neutron cross-section, half-life and gamma-ray abundance). For many elements and applications, NAA offers sensitivities that are superior to those attainable by other methods. Using this technique, elemental concentrations of the order of parts per billion or better are obtainable. In addition, because of its accuracy and reliability, NAA is generally recognized as the "referee method" of choice when new procedures are being developed or when other methods yield results that do not agree (Glascock, 1996).

The NAA has many advantages, some of which include among others:

- Measures the total amount of an element in a material without regard to its chemical or physical form.
- It is non-destructive, in that, the integrity of the sample is not changed in any manner before irradiation – thus, the problem of reagent–introduced contaminants in completely avoided.

- It is multi-elemental analytical technique in that many elements can be analyzed simultaneously in a given sample, without changing on altering the apparatus as is the case in atomic absorption.
- It has an inherent potential for accuracy compared to other analytical techniques. Since the theoretical basis of NAA is simple and well understood, the source of uncertainties can be modelled and well estimated.

The NAA has numerous applications in varied fields of study, one of which is in the experimental determination of neutron-induced activation cross section data.

A database of activation cross sections for neutron energies (of up to 20MeV) is required for the design of a D-T fusion reactor, neutron dosimetry and neutron shielding in a reactor facility, and for confirming predictions based on reaction calculations. The (n, γ) cross section σ_0 is a basic constant and the reliability of the literature data should be a matter of concern; as the accuracy and consistency of σ_0's from different libraries are often troublesome (De Corte et al 1988) thus making a selection of reliable data difficult. A number of cross section data have been compiled in several evaluated data libraries, such as Japanese Evaluated Nuclear Data Library, JENDL-3.3 (Shibata et. al., 2002), Evaluated Nuclear Data File, ENDF/ B-VI (Rose, 1991), European Joint Evaluated File, JEF (2000), Russian Evaluated Library, BROND (2000), and the IAEA Fusion Evaluated Nuclear Data Library, FENDL, but they are evaluated mainly on the basis of theoretical calculations. Experimental data, if available, are used to normalize the calculated values and to improve their accuracy and reliability. In cases where no measurements have been made, the systematics for the majority of the reactions are used to predict the cross sections.

In order to use a neutron source for neutron data measurements, there is the need to have an accurate knowledge of the neutron spectrum parameters. The Nigeria Research Reactor-1, NIRR1, is designed for use in NAA thus, its neutron flux remains stable and constant during both irradiations of the 'bare' and the 'Cd-covered' foils. The need for a careful and complete characterization of the neutron flux parameters in the irradiation channels is to optimize its utilization for NAA via relative, absolute and single comparator methods, especially, the k_o-method. The method is widely accepted for multi-element NAA with respect to variations in neutron spectrum parameters and gamma-ray counting geometry (De Corte, F, 1987). The k_0-standardized method, developed in the 1970s by Simonits et al., (1975) involves the simultaneous irradiation of a sample and a neutron flux monitor, such as gold, and the use of a composite nuclear constant called k_0-factor. The k_0-factor is independent of irradiation and measuring conditions thus, eliminating the problems of non-availability of standards for certain elements and the inaccuracy caused by poorly prepared in-house standards (Jonah et al, 2005).

The neutron spectrum parameters are needed in the equation for concentration calculation based on the k_0 – standardization method by the use of the Hogdahl convention for the so–called "1/v" nuclides. The parameters are: the shape factor of the epithermal neutron flux, α, approximated by a $1/E^{1+\alpha}$ distribution and the thermal to epithermal neutron flux ratio, *f*. The value of α can be positive or negative depending on the reactor configuration, which corresponds to a 'softened' or a 'hardened' epithermal neutron spectrum compared to the ideal one (De Corte et al, 1982). The knowledge of α is essential for the correction of resonance integrals I_0 (equivalent of epithermal neutron cross section), i.e. for the conversion of I_0 values to I_0 (α) values for its use in actual $1/E^{1+\alpha}$ epithermal

neutron spectrum. Much attention is given to the determination of the epithermal neutron flux shape factor α and the subcadmium-to-epithermal neutron flux ratio *f*, since these two parameters vary from one reactor to another as well as among the different irradiation sites in a given reactor. The "Cd-ratio for multi-monitor" method, for reactors with stable neutron flux, has been recommended for neutron flux monitoring. Moreover, the method has been adjudged the most accurate for α-monitoring (De Corte et al, 1981). The experimental methods for the determination of neutron flux parameters required in both the Hogdahl convention and the Wescott formalism (deviation from the 1/v dependence) have been enumerated in several published works (De Corte et al, 1994).

1.2 Review of previous works

Low-power research reactors such as the Canadian SLOWPOKE and the Chinese Miniature Neutron Source Reactor (MNSR) exhibit stable neutron flux characteristics, which make them suitable for NAA via the k_0-standarndized method (Kennedy et. al., 2000; Akaho et al, 2002; Acharya et al, 2003). Recently, (Jonah *et al,* 2005) determined the thermal to epithermal flux ratio *f*, and the epithermal flux shape factor α, associated with an inner irradiation channel B2 and an outer irradiation channel B4 of the NIRR-1 (Jonah et al, 2005) out of the six (four inner and two outer) irradiation channels connected to the two pneumatic transfer systems A and B. The experimental methods for the determination of these parameters via both the Hogdahl convention and the Westcott formalism have been enumerated in several publications (De Corte et al, 1994; Kennedy et. al, 2000; Akaho et al, 2002; Acharya et al, 2003; De Wispelaere et al, 2003; Jonah et al, 2005).

In recent past, a number of investigations were conducted to measure activation cross sections σ_0 and isomeric cross section ratios I_0 of some nuclides whose σ_0 and I_0 are

either doubtful or have never been measured (Andrej, T., 2002). More recently, the IAEA set up the Working Party on Evaluation Co-operation (WCEC) Subgroup-23 (SG-23) to assemble, verify and validate an evaluated data library for the minor fission products by reviewing and making use of existing evaluations, running nuclear model calculations and performing partial re-evaluation work (Andrej, T., 2002). The purpose of the exercise was to compare the thermal capture cross sections and resonance integrals from the SG-23 library to the equivalent values in the k_0 database. It was discovered that 12 out of 30 nuclides studied showed differences from 5% to greater than 20%.

1.3 Present work

The main objective of this work is to determine some discrepant cross section data in the framework of the IAEA Coordinated Research Project No.13728 entitled "Reference Database for NAA" using the NIRR-1 Facilities. In this respect, the following specific objectives are to be performed.

i. Calibration of the NIRR-1 High Purity Germanium, HPGe, detector by a semi-empirical method.

ii. The determination of the epithermal neutron shaping parameter α, and the thermal to epithermal flux ratio *f*, of the irradiation sites A1 an A2 of NIRR-1.

iii. The determination of magnitudes of the thermal, epithermal and fast neutrons flux in the irradiation sites A1 and A2.

iv. The determination of Maxwellian neutron temperature T_n and Modified Spectral Index r $(\alpha)\sqrt{T_n / T_0}$ of the irradiation sites A1 and A2.

v. The determination of thermal neutron cross section σ_0, and/or resonance integral I_0, for nuclides with discrepant data.

vi. Comparison of results with data from literature.

1.4 Outline of Work

The theoretical framework of neutron and gamma interaction with matter is presented in chapter two. The description of materials, instrumentation and the experimental facilities used are discussed in chapter three. In chapter four, the results of Calibration of HPGe detector, epithermal neutron shaping parameter α, the thermal to epithermal flux ratio *f*, of the irradiation sites A1 and A2 of NIRR-1, Westcott's $g(T_n)$ factor, Maxwellian neutron temperature T_n, Modified Spectral Index $r(\alpha)\sqrt{T_n/T_0}$, Resonance Integral and thermal neutron cross sections σ_0, for the nuclides with discrepant data are presented, discussed and compared with results from the literature and nuclear data libraries. Conclusion and recommendation are presented in chapter five.

CHAPTER TWO

THEORETICAL FRAMEWORK

2.0 Neutrons

Although there are several types of neutron sources (reactors, accelerators, and radioisotopic neutron emitters) one can use for NAA, nuclear reactors with their high fluxes of neutrons from uranium fission offer the highest available sensitivities for most elements. Types of reactors and positions within a reactor can vary considerably with regard to their neutron energy distributions and fluxes, due to the materials used to moderate (or reduce the energies of) the primary fission neutrons. However, as shown in Figure 2.1, most neutron energy distributions are quite broad and consist of three principal components (thermal, epithermal, and fast).

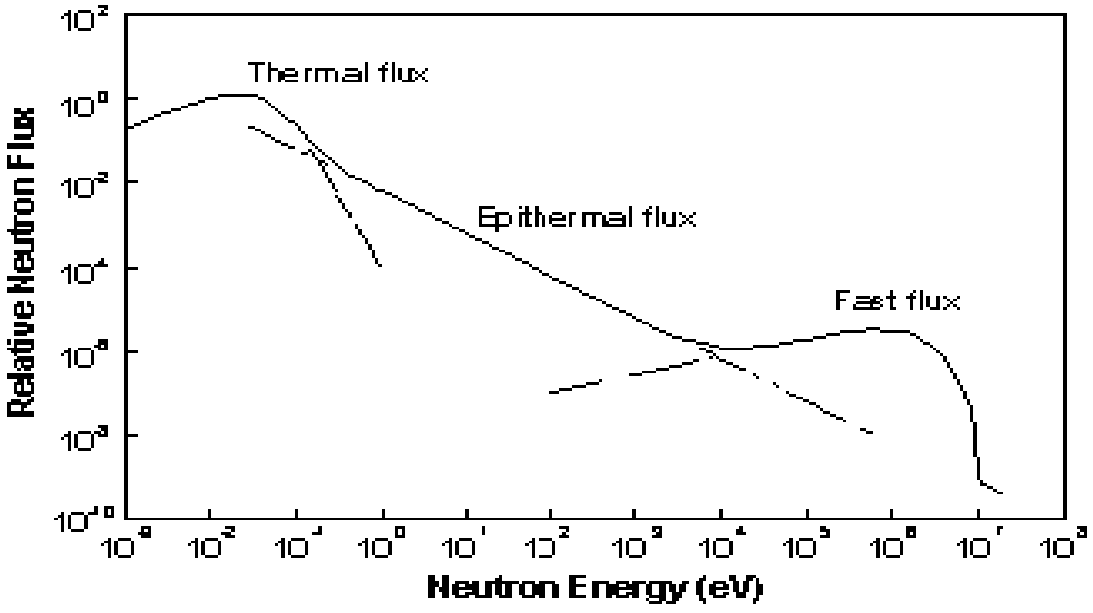


Fig. 2.1 A typical reactor neutron energy spectrum showing the various components used to describe the neutron energy regions.

The thermal neutron component consists of low-energy neutrons (energies below 0.5 eV) in thermal equilibrium with atoms in the reactor's moderator. At room temperature, the energy spectrum of thermal neutrons is best described by a Maxwell-Boltzmann distribution with a mean energy of 0.025 eV and a most probable velocity of 2200 m/s. In most reactor irradiation positions, 90-95% of the neutrons that bombard a sample are thermal neutrons. In general, a one-megawatt reactor has a peak thermal neutron flux of approximately 1 x 10^{13} neutrons per square centimeter per second (Glascock, 1996).

The epithermal neutron component consists of neutrons (energies from 0.5 eV to about 0.5 MeV) which have been only partially moderated. A cadmium foil 1 mm thick absorbs all thermal neutrons but will allow epithermal and fast neutrons above 0.5 eV in energy to pass through. In a typical unshielded reactor irradiation position, the epithermal neutron flux represents about 2% of the total neutron flux. Both thermal and epithermal neutrons induce (n, γ) reactions on target nuclei. An NAA technique that employs only epithermal neutrons to induce (n, γ) reactions by irradiating the samples being analyzed inside either cadmium or boron shields is called epithermal neutron activation analysis (ENAA).

The fast neutron component of the neutron spectrum (energies above 0.5 MeV) consists of the primary fission neutrons which still have much of their original energy following fission. Fast neutrons contribute very little to the (n, γ) reaction, but instead induce nuclear reactions where the ejection of one or more nuclear particles - (n, p), (n, n'), and (n, 2n) - are prevalent. In a typical reactor irradiation position, about 5% of the total flux consists of fast neutrons. An NAA technique that employs nuclear reactions induced by fast neutrons is called fast neutron activation analysis (FNAA). However, the flux distributions of thermal, epithermal and fast neutrons in the irradiation positions of compact

low-power research reactors such as the miniature neutron source reactor (MNSR) deviate from the general characteristics enumerated above (De Corte, 1981).

2.1.0 Neutron Interaction with Matter

Neutron interaction can be classified as absorption and scattering reactions.

2.1.1 Absorption

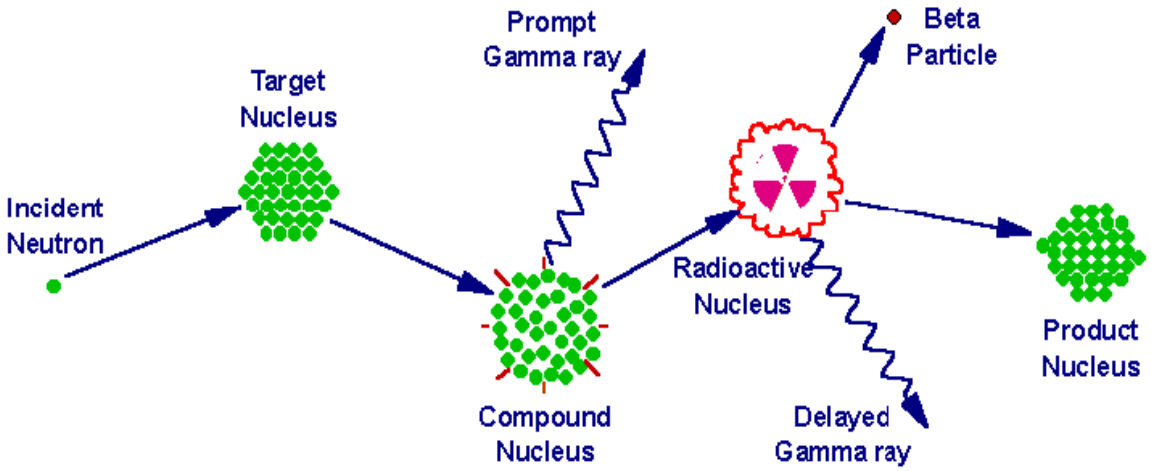


Fig 2.2 Diagram illustrating the process of neutron capture by a target nucleus followed by the emission of gamma rays.

The most common type of nuclear reaction used for NAA, namely the neutron capture (radiative capture) or (n,γ) reaction is illustrated in Figure 2.2. When a neutron interacts with the target nucleus via a non-elastic collision, a compound nucleus is formed, in an excited state. The excitation energy of the compound nucleus is due to the binding energy of the neutron with the nucleus. The compound nucleus will almost instantaneously de-excite, within about 10^{-12} seconds or less, into a more stable configuration through emission of one or more characteristic prompt gamma rays. In many cases, this new

configuration yields a radioactive nucleus which also de-excites (or decays) by emission of one or more characteristic delayed gamma rays, but at a much slower rate according to the unique half-life of the radioactive nucleus. Depending upon the particular radioactive species, half-lives can range from fractions of a second to several years.

Other reactions that involve neutron interaction and the formation of an unstable compound nucleus are (n, p), (n, α), (n, n$^{/}$), (n, 2n) and (n, p). These groups of reactions are known as threshold reactions. They require neutrons above a minimum energy in order to take place at all. Each material with a different threshold will respond to a somewhat different range of neutron energy.

In the (n, n$^{/}$) process, the expelled particle is a neutron with much lower energy than the captured neutron. The overall effect is that energy is transferred from the incident neutron to the target nucleus. Practically all this energy is given out in form of gamma radiation from the compound nucleus. Thus, the (n, n$^{/}$) reaction is usually referred to as inelastic scattering. These types of reactions, in which there is no net loss of neutrons, are generally not included when neutron absorption is discussed.

2.1.2 Scattering

When a neutron collides with a target nucleus and transfers part or all of its kinetic energy to the target, without being absorbed by the target, the process is known as scattering. Scattering may be inelastic or elastic, depending on whether the energy loss suffered by the incident neutron is partly spent on exciting the target nucleus or is merely transferred to the target without changing form. Inelastic scattering has been described as the (n, n$^{/}$) capture reaction.

Elastic scattering is by far the dominant mode of interaction for neutrons with energies from around 10MeV down to epithermal energy of about 1eV. In this type of interaction, the kinetic energy of the neutron is partially transferred to the target nucleus, thereby slowing down the neutron and changing its course due to the collision. The maximum amount of energy that can be transferred depends only on the mass of the nucleus that is participating in the collision. The smaller the participating nucleus, the greater the energy transferred. Since both kinetic energy and momentum are conserved in elastic scattering, it can be shown that the maximum possible energy transfer resulting from a head-on collision is

$$E_1 - E_2 = \frac{4A}{(A+1)^2} E_1 \qquad 2.01$$

where E_1 and E_2 are the respective energies of the neutron before and after collision; A is the relative atomic weight of the nucleus, which can be considered equal to its mass number; and the relative mass of the neutron is considered unity.

It follows from equation 2.01 that a neutron can lose all of its kinetic energy in a single head-on collision with the hydrogen nucleus. This is the reason why water, paraffin and other hydrogenous materials are used as neutron moderators.

2.1.3 Neutrons Reaction Cross-Sections

Reaction cross-section is a quantitative measure of the probability of occurrence of a given neutron-induced reaction. For thermal neutrons, the cross section is usually expressed in barns (1 barn = 10^{-24} cm^2) while for fast neutrons it is within the range of millibarns. Cross sections are energy dependent, varying almost inversely with velocity v

of the incident neutron. Thus the cross-section of a given target nucleus for a given type of reaction depends on the neutron energy.

When only one single nucleus is referred to, its cross-section is known as the microscopic cross-section and is conventionally denoted as $\sigma(x, i)$. The suffixes refer to the reaction type and nucleus respectively.

When a medium is considered, the total cross-section of its nuclei per unit volume is called the macroscopic cross-section, denoted by Σ. It is generally defined as

$\Sigma = N\sigma \times 10^{-24} cm^{-1}$, where σ is in barns for the corresponding type of reaction and N is the total number of nuclei in a unit volume. Since N can be found from Avogadro's number, the macroscopic cross section for a medium of only one type of isotope is (IAEA, 1970).

$$\Sigma = \frac{\rho N_A \sigma}{A} \times 10^{-24} = \frac{0.602 \rho \sigma}{A} cm^{-1} \qquad 2.02$$

where A is the mass number of the isotope and ρ is the density of the medium in g/cm^3. In most cases, the σ value is usually given for an element, and not for its isotopes. In such cases the above equation is valid, provided that A is taken as the atomic weight of the element, and Σ is then the macroscopic cross-section of the material.

However, in practice the medium of interest comprises several elements. Now assuming such medium to be homogeneous, the cross section for a given type of reaction at certain energy is the weighted contributions of all elements present. The general equation for medium comprising m elements is

$$\Sigma = N_1\sigma_1 + N_2\sigma_2 + \ldots\ldots\ldots\ldots N_m\sigma_m = \sum_{i=1}^{i=m} N_i \sigma_i \qquad 2.03$$

where N_i is the number of nuclei of element i per cm^3 of the medium and σ_i is its microscopic cross section. Now supposing that the weight percentage, w_i, of each constituent element is known, then the equation 2.03 becomes.

$$\Sigma = 6.02 \times 10^{-3} \rho \sum_{i=1}^{i=m} \frac{w_i \sigma_i}{A_i} \qquad 2.04$$

with $$w_i = \left(\frac{g \Gamma_\gamma \Gamma_n}{\Gamma} \right)_i \frac{1}{E_{r,i}^2} \qquad 2.04b$$

where g is the statistical weight factor, Γ_γ is the radiative width, Γ_n is the neutron width, and Γ is the total width of resonance.

2.2 Interaction of Radiation with Matter

Radiation interacts with matter and losses energy in various ways. These interactions depend on the type of radiation i.e. whether the radiation is particulate or non- particulate or whether it is charged or uncharged (Leo, 1987 and Singru, 1972).

2.2.1 Charged Particle radiation

2.2.1.1 Electrons

There are three important processes by which electrons lose energy during their passage through matter.

i. *Inelastic Collision:* In this kind of collision, the incident electron transfers part of its energy to a bound electron (excitation) or an unbound electron (ionization). The mean energy loss due to inelastic collision for electron energies, $E < m_o c^2$, is given (Singru, 1972) by:

$$\frac{dE}{dx} = \frac{4\pi e^4 nZ}{m_0 v^2} Ln \frac{1.16 m_0 v^2}{2I} \qquad 2.05$$

where n is the number of atoms per unit volume, Z is the atomic number of the absorber, e is the charge, m_0 is the rest mass of the electrons and I is the mean excitation energy of the atomic electrons.

ii. *Elastic Collisions:* The incident electron can have an elastic collision with a nucleus resulting in a deflection of the electron without any radiative loss or excitation of nucleus. The cross section for this process is of the order of (e^2/m_0v^2) and it increases with Z^2, where v is the velocity of the incident electron.

For practical purposes, the total energy loss per unit length of the electrons is the sum of ionization and radiative loss, i.e.

$$\left(\frac{dE}{dx}\right)_{Total} = \left(\frac{dE}{dx}\right)_{ion} + \left(\frac{dE}{dx}\right)_{rad} \qquad 2.06$$

The ratio of specific energy losses is given approximately by (Singru, 1970).

$$\frac{\left(\frac{dE}{dx}\right)_r}{\left(\frac{dE}{dx}\right)_i} \cong \frac{EZ}{700} \qquad 2.07$$

Where E is the electron energy in MeV and Z is the atomic number of the absorber. It could therefore be seen that losses due to radiation are always a small fraction of the energy losses due to ionization and excitation and are significant only in absorber materials of high atomic number.

i. *Bremstrahlung:* Incident electron passing through a field of a nucleus experiences a deflection with a resultant emission of radiation. The process is known as bremstrahlung. This leads to loss of kinetic energy of the incident electron. This can be considered as a radiant type of inelastic collision between the electron and an atomic nucleus. The rate of energy loss in this interaction is proportional to $Z^{2,}$ where Z is as defined. The rate of such radiation loss is given by (Singru, 1972)

$$\left(\frac{dE}{dx}\right)_r \propto \frac{Z^2 n}{A\left[E + m_0 c^2\right]} \qquad 2.08$$

where E is the energy of the electron, A is the mass number of the absorber and n is the atomic density.

2.2.1.2 Positrons

The interaction of positron with matter is almost identical with that of electron but for some minor differences. However, there is a very important way in which positron can annihilate with the electron in matter. This annihilation can either be a free annihilation with an electron via the formation of (e, e) hydrogen-like quasistable combination known as positronium. The positron annihilation leads to two photons if electron-positron spin is anti-parallel and to three photons if the spin orientation is parallel.

2.2.1.3 Heavy Charged Particles

Heavy charged particles (protons and alpha) lose their energy mostly by ionizing the atoms of the material they pass through. The heavy charged particle gives up its kinetic energy to the atoms of the absorber. The electron of the absorber atom will either get excited to a higher level or leave the atom depending on the energy gained by it. At any given time the particle is interacting with the many electrons, so the net effect is to continuously decrease its velocity until the charged particle stops.

The linear stopping power, S (E) is defined as the amount of energy loss over unit length of the particle. The S (E) for charged particles in a given absorber is (Singru, 1972):

$$-\frac{dE}{dx} = \frac{4\pi (Ze^2)^2 Zn}{m_0 v^2}\left[Ln\left(\frac{2m_0 v^2}{I}\right) - Ln\left(1-\beta^2\right) - \beta^2\right] \qquad 2.09$$

where n, Z, I, E, Ze and v are the number of atoms per unit volume of the absorber, atomic number of the absorber, average minimum excitation energy of the atom, kinetic energy, charge and velocity of the ionizing particle respectively.

2.2.2.1 Uncharged Particle Radiation

2.2.2.2 Electromagnetic Radiation

Although gamma rays interact with matter in many different ways, only three major types of interactions play an important role in radiation measurement: photoelectric effect, Compton scattering and pair production.

2.2.2.1.1 Photoelectric Effect

In the photo-electric effect the incident γ-ray interacts with an absorber atom, the γ-ray disappears. In its place an energetic photoelectron is ejected by the atom from one of its bound shells. The interaction is with the atom as a whole and cannot take place with free electrons. The kinetic energy (K_e) of the emitted photoelectron is given by (Knoll, 1979).

$$K_e = h\nu - E_b \qquad 2.10$$

where $h\nu$ is the energy of the incident photon and E_b is the binding energy of the photoelectron in its original shell. The photoelectron could be emitted from the atom only if $h\nu > E_b$.

This process is the predominant mode of interaction for gamma rays (or x–rays) of relatively low energy (Knoll, 1979), and it is also enhanced for absorber materials of high atomic number, Z. The probability of photoelectric absorption per atom over all ranges of energy, E and atomic number Z is approximately (Evans, 1982)

$$\tau \cong cons\tan t \times \frac{Z^n}{E_\gamma^{3.5}} \qquad 2.11$$

where the exponent n varies between four and five over the gamma ray energy region of interest. This severe dependence of the photoelectric absorption probability on the atomic number of the absorber is a primary reason for the preponderance of high Z materials used as gamma ray shield. (Knoll, 1979; Singru, 1974)

2.2.2.1.2 Compton Effect

This is also known as the Compton scattering. It is the inelastic scattering of a photon by an electron in which both energy and momentum are conserved. It is the predominant interaction mechanism for gamma ray energies typical of radioisotope sources. The photon transfers a portion of its energy to the recoil electron. The expression that relates the energy transfer and the scattering angle for any given interaction is

$$h\nu' = \frac{h\nu}{1 + \frac{h\nu}{m_o c^2}(1 - \cos\theta)} \qquad 2.12$$

where hύ is the energy of the scattered photon; hν is the energy of the incident photon; $m_o c^2$ is the rest- mass energy of the electron (0.511 MeV) and θ is the scattering angle of the photon.

The probability of Compton scattering per atom of the absorber depends on the number of electrons available as scattering targets and therefore increases linearly with Z. This probability is also large only for photons with a low energy, that is, in the region in which photoelectric absorption is the main contributor to all interaction processes.

2.2.2.1.3 Pair Production

When a gamma ray photon having energy greater than 1.02 MeV (twice the electron's rest mass energy) strikes a material of high atomic number, the photon is completely absorbed and an electron-positron pair is produced. This process is known as pair production and the threshold energy of the photon is 1.02 MeV. Therefore, this process is predominantly restricted to high-energy gamma rays.

2.3 Theory of Activation Analysis

The neutron activation analysis is mostly carried out using thermal neutrons through the (n,γ) reactions. When a neutron is captured by a target nuclide X in a reaction known as neutron capture, the reaction could be represented by the equation:

$$ {}^{A}_{Z}X(n,\gamma)^{A+1}_{Z}X \qquad 2.13 $$

Suppose a target with N nuclei per cm^3 is placed in a neutron beam flux, ϕ (neutrons/cm^2s), then the number of interactions per second is given by:

$$ \phi.\sigma.\ N\ (cm^{-3}s^{-1}) \qquad 2.14 $$

Then ,the cross-section σ can be defined as:

$$ \sigma(cm^2) = \frac{Number\ of\ \text{int}\ eractions(cm^{-3}s^{-1})}{\phi(cm^{-2}s^{-1})N(cm^{-3})} \qquad 2.15 $$

Therefore, the (n,γ) reaction rate per nucleus (interactions /s) is given by:

$$ R = \phi.\sigma \qquad 2.16 $$

However, in general eq. 2.16 may be written in the form

$$ R = \int_0^\infty \sigma(v)\phi'(v)dv = \int \sigma(E)\phi'(E)dE \qquad 2.17 $$

where

$\sigma(v)$ = (n,γ) cross section at neutron velocity, v

$\sigma(E)$ = (n,γ) cross section at neutron energy, E

$\phi^{/}(v)$ = neutron flux per unit of velocity interval (in cm^{-3}) at neutron velocity, v

= $n^{/}(v)v$, with $n^{/}(v)$ being the neutron density per unit of velocity interval (in cm^{-4} s) at neutron velocity, v.

$\phi^{/}(E)$ = neutron flux per unit of energy interval (in $cm^{-2}\ s^{-1}\ eV^{-1}$) at neutron energy, E.

In equation 2.17, $\sigma(v) = \sigma(E)$ and $\phi^{/}(v)dv = \phi^{/}(E)dE$ with $E = \frac{1}{2}\ m_n v^2$, where m_n is the neutron rest mass. The functions $\sigma(v) = \sigma(E)$ and $\phi^{/}(v)$ or $\phi^{/}(E)$ are complex, and depend on the (n,γ) reactions and irradiation site respectively. Fortunately, introduction of some generally valid characteristics yields the possibility of avoiding the actual integration and of describing accurately, the reaction rate in a relatively simple way by means of the so called formalisms or convention. These characteristics are:

- The (n,γ) cross-section $\sigma(v)$ versus v has been shown to vary as 1/v, that is $\sigma(v) \sim 1/v$ dependence or $\sigma(E)$ versus E as a $\sigma(E) \sim 1/E^{1/2}$ dependence. Above the thermal energy region, the cross section shows some complex behavior known as resonance: Within this resonance region (Fig 2.3), the cross section obeys the Breit- Weigner one level formula (Breit and Weigner, 1936). It is important to note that only a few (n,γ) reactions of interest in NAA show significant deviation from the 1/v – dependence in the energy region below 1.5 eV (due to low-lying resonance).These deviations are accounted for by multiplying eq. 2.17 by a factor $g(T_n)$, known as Wescott correction factor. This factor depends on neutron temperature T_n.

❖ The neutron flux distribution $\phi'(E)$ versus E, can be subdivided into three components (Fig. 2.1):

i. A fission (fast) neutron spectrum, which has a continuous energy distribution with a maximum higher than 10MeV, is described by Watt's empirical equation (Hoste, 1988):

$$n(E) = 0.7725\, E^{1/2} \exp(-0.775E) \qquad 2.18$$

However, the contribution of this group of neutrons (above 1MeV) to (n,γ) reactions is usually small and may be neglected. They however give rise to threshold reactions e.g. (n, n'), (n, p), (n, α), (n, 2n) and can cause interference as in the determination of aluminum by the ^{27}Al (n, γ) ^{28}Al reaction, where the presence of silicon can give rise to positive errors due the ^{28}Si (n, p) ^{28}Al reaction.

ii. Thermal neutrons, which are low energy neutrons, arise from successive collisions of high energy neutrons with the moderator atoms in a process known as thermalization. These neutrons which are in thermal equilibrium with the atoms of the moderator obey Maxwell-Boltzmann distribution (IAEA, 1970).

In $\phi(E)$ versus E (fig.2.3b) or n'(v) versus v curve, the most probable neutron energy at 20°C obtained from $E_n=kT$ is 0.025eV corresponding to neutron velocity of 2200 m/s. Different reaction conventions have been applied to describe the reaction rate for (n,γ) reactions, such as those developed by Wescott (De Corte et al, 1987) and by Stoughton and Halperin (De Corte et al, 1987). However the most practical version for activation analysis is probably

the one proposed by Hϕgdahl (De Corte, 1987and Hoste, 1988), which is valid if:

$$\sigma(v) \cong 1/v \qquad 2.19$$

This is the case for almost all nuclides of interest in activation analysis.

iii. the epithermal neutron spectrum can be described in the ideal case by a

$$\phi_e^{'}(E) \cong \frac{1}{E} \qquad 2.20$$

dependence. However, in actual irradiation sites, equation .2.20 can be replaced by

$$\phi_e^{'}(E) \cong \frac{1}{E^{1+\alpha}} \qquad 2.21$$

with α is greater or less than zero, being to a first approximation, independent of neutron energy (De Corte, 1987).

The neutron flux and reaction rate could be divided into two parts using a Cd – filter. Thus, a sample irradiated under Cd is only activated by epithermal neutrons, and the conventional sub-cadmium flux (ϕ_s) is the sum of the conventional Maxwellian flux plus part of the epithermal flux up to energy of the cadmium cut-off.

Thus by irradiating a nuclide under Cd- cover the (n,γ) reaction rate is drastically reduced in the low energy region, where the neutrons are largely absorbed by the Cd- due to the very high Cd (n, γ) cross-section, resulting from the ^{113}Cd (n, γ) ^{114}Cd resonance at 0.178 eV, as depicted in Fig 2.4a.

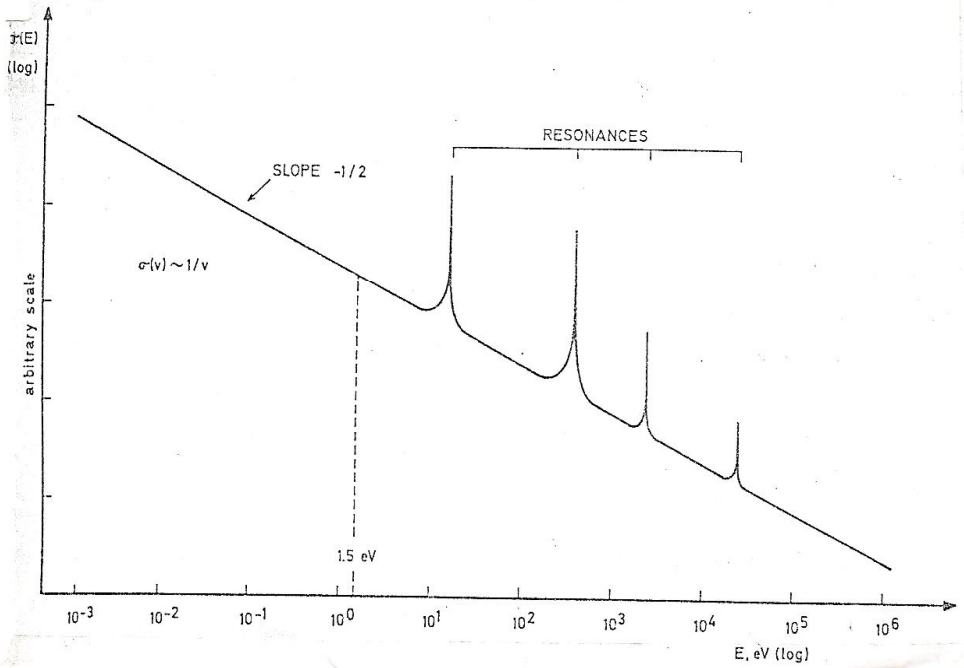


Fig. 2.3a Schematic representation of the (n, γ) cross-section function σ(E) versus E (De Corte, 1987)

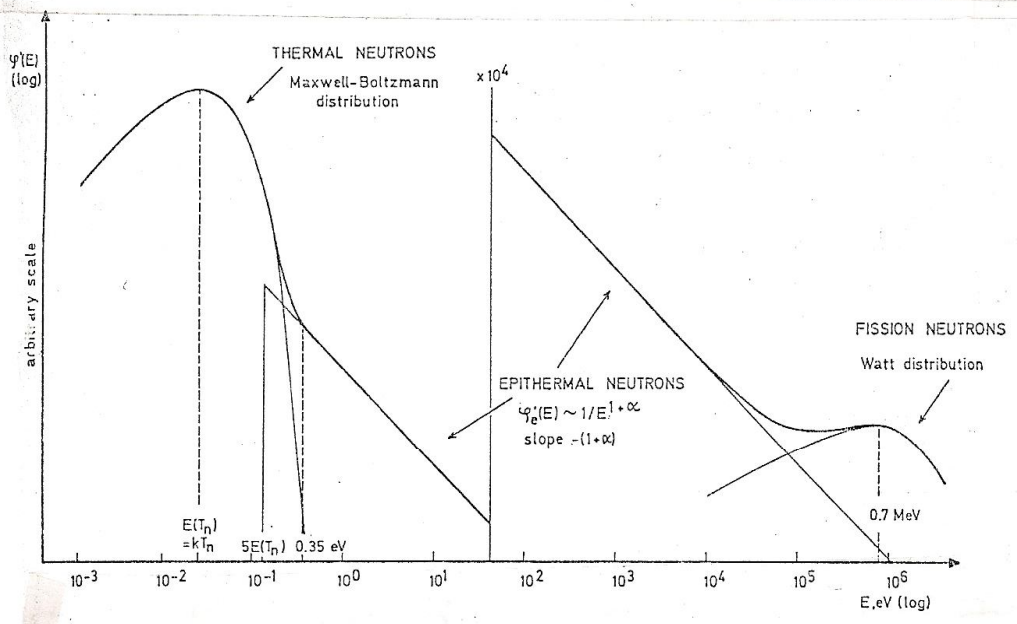


Fig. 2.3b. Schematic representation of the reactor neutron flux distribution φ'(E) versus E (De Corte,1987)

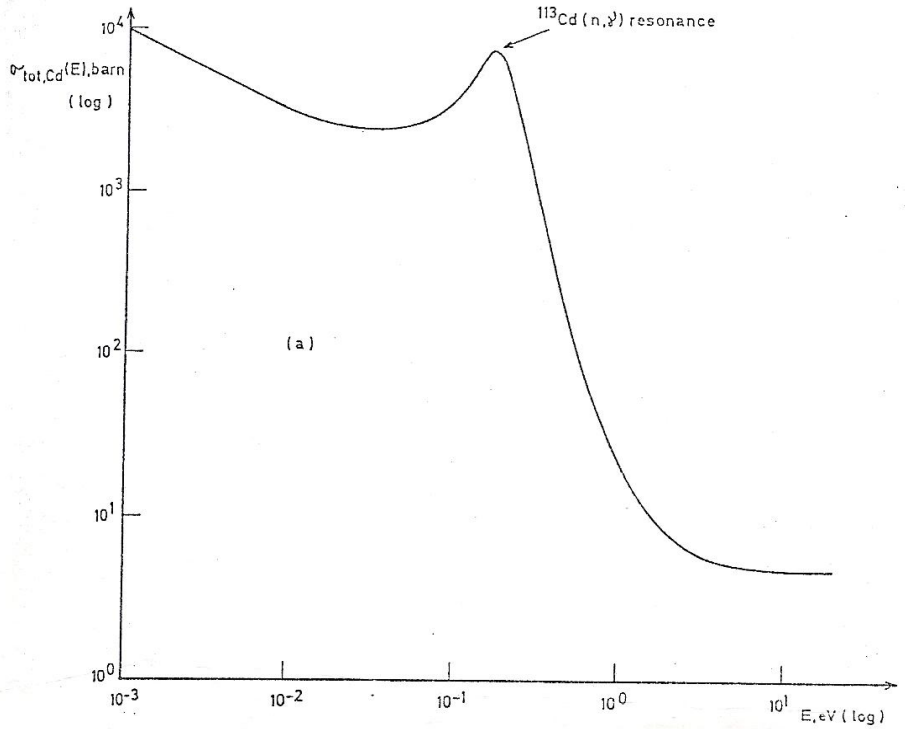


Fig. 2.4a Cd total cross section curve, $\sigma_{tot,Cd}(E)$ versus E (De Corte, 1987)

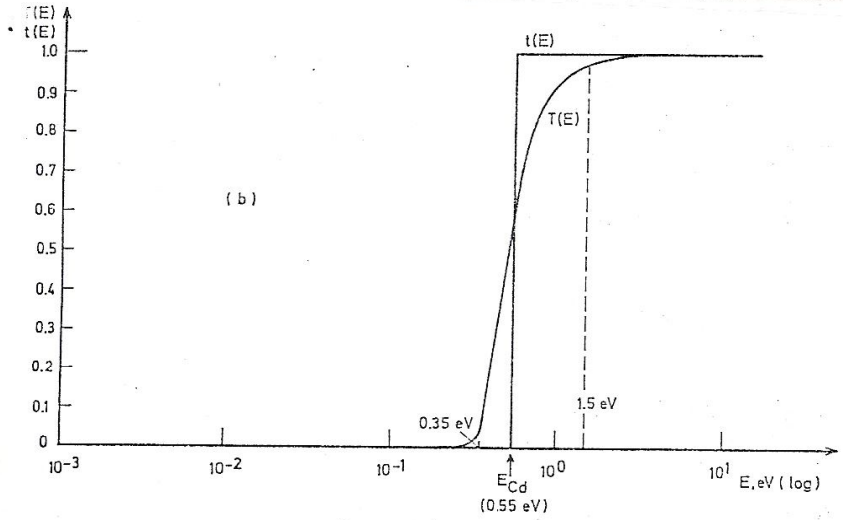


Fig. 2.4b. Actual and idealized Cd neutron transmission functions, T(E) and t(E) versus E (De Corte,1987)

The transmission function versus energy under cadmium cover is shown in Fig 2.4b. It is represented by

$$T(E) = \exp -(\sigma_{tot,cd}(E)\delta N_A I_0 / M) \qquad 2.22$$

with δ = density of Cd (8.642g/cm^3, De Corte F., 1987)

N_A = Avogadro's number (6.02 x 10^{23}mol^{-1})

I_0 = Cd- thickness (0.1cm)

M = Molar mass of Cd (112.41gmol^{-1})

σ_{tot}, Cd = cross section function (see Fig 2.4b), in cm^2, where T (E) $\cong$0 for E< 0.2 eV and T (E) $\cong$ 1 for E> 2eV

In obtaining the T (E) curve of Fig 2.4b, it was assumed that the geometry effects caused by sample and Cd- cover were negligible and that a mono-directional beam of neutrons was hitting a 1 mm- thick Cd –foil in a direction normal to its face. Thus by defining an idealized transmission as a step function t (E), situated at the so-called Cd- cut-off energy, E_{cd} (with t (E) = 0 at E=E_{cd} and t (E) = 1 at E>E_{cd}), so that the epicadmium reaction rate R_e may be written as:

$$R_e = \int_0^\infty \sigma(E)\phi'(E)T(E)dE = \int_0^\infty \sigma(E)\phi'(E)t(E)dE = \int_{E_{cd}}^\infty \sigma(E)\phi'(E)dE \qquad 2.23$$

Internationally a value 0.55eV has been accepted as the standard value of E_{cd} under the following conditions:

i. The nuclide should be the type that obeys Hϕgdahl convention

ii. The neutron flux should be homogeneous and isotropic, with an epithermal neutron flux distribution obeying the 1/E – law down to 0.35 eV (where T (E) approaches zero; see Fig 2.4b)

iii. The irradiated material should have a relatively small volume and should be positioned approximately in the centre of a cylindrical Cd – box with 1mm wall thickness and a height /diameter ratio =2.

Thus according to Hϕgdahl convention, Eq. 2.16 with the introduction of the E_{cd}-concept is split into:

$$R = \int_0^{v_{cd}} \sigma(v)\phi'(v)dv + \int_{E_{cd}}^{\infty} \sigma(E)\phi'(E)dE \qquad 2.24$$

with $v_{cd} = (2E_{cd}/M_n)^{1/2}$ 2.25

Since $\sigma(v) \sim 1/v$ up to v_{cd}, then $\sigma(v) = \sigma_0 v_0/v$, where the set v_0 and σ_0 is arbitrarily chosen. Since also one can assume an undisturbed flux, $\phi'_e(E) \sim 1/E^{1+\alpha}$ (or $\phi'_e(E) \sim 1/E$, if $\alpha = 0$) epithermal spectrum down to E_{cd}, in fact down to 0.35 eV, one can write:

For a 1/E Spectrum

$\phi'(E) = \phi_e'(1\,eV)\ 1eV/E$ 2.26

where 1eV is an arbitrary chosen reference energy. By defining the conventional epithermal neutron flux ($cm^{-2}s^{-1}$) as:

$$\phi'(E) = \phi_e(E)/E, \text{ thus, } \int_{E_i}^{E_f} \phi_e'(E)dE = \phi_e \int_{E_i}^{E_f} \frac{1}{E}dE = \phi_e Ln(E_f/E_i) \qquad 2.27$$

ϕ_e is called the true epithermal neutron flux per unit ln E interval, since integration of Eq. 2.27 yields

$$\phi_e = \left[\int_{E_i}^{E_f} \phi_e'(E)dE\right] / \left[Ln(E_f/E_i)\right] \qquad 2.28$$

with E_i and E_f being the low and high boundaries of the epithermal spectrum. But $\phi'(v) = n'(v)\, v$, then Eq. 2.24 can be written as:

$$R = \sigma_0 v_0 \int_0^{v_{cd}} n'(v)dv + \phi_e(1eV)\int_{E_{cd}}^{\infty} \sigma(E)dE/E = \sigma_0 v_0 n_s + \phi_e I_0 = \phi_s \sigma_0 + \phi_e I_0 \qquad 2.29$$

where I_0 is the resonance integral for 1/E spectrum, given by

$$I_0 = \int_{E_{cd}}^{\infty} \sigma(E)dE/E \qquad 2.30$$

and $n_s = \int_0^{\infty} n'(v)dv$ is the sub cadmium neutron density (cm^{-3}), and $\phi_s = v_0 n_s$, is the conventional sub cadmium (thermal) neutron flux ($cm^{-3}s^{-1}$).

For $1/E^{1+\alpha}$ spectrum

$$\phi_e'(E) = \phi_e'(1eV)1eV^{1+\alpha}/E^{1+\alpha} = \phi_e 1eV/E^{1+\alpha} \qquad 2.31$$

ϕ_e is the (true) epithermal neutron flux per unit $(-E^{\alpha}/\alpha)1eV^{\alpha}$ interval, since integration of Eq. 2.30 yields

$$\phi_e = \left[\int_{E_i}^{E_f} \phi_e'(E)dE\right] / 1eV^{\alpha}\left[-E^{-\alpha}/\alpha\right]_{E_i}^{E_f} \qquad 2.32$$

Hence,

$$\begin{aligned} R &= \sigma_0 v_0 \int_0^{v_{cd}} n'(v)dv + \phi_e 1eV^{\alpha}\int_{E_{cd}}^{\infty} \sigma(E)dE/E^{1+\alpha} \\ &= \sigma_0 v_0 n_s + \phi_e I_0(\alpha) = \phi_s \sigma_0 + \phi_e I_0(\alpha) \end{aligned} \qquad 2.33$$

with $I_0(\alpha)$, the resonance integral for a $1/E^{1+\alpha}$ spectrum (cm^2), given by:

$$I_0 = 1eV^{\alpha}\int_{E_{cd}}^{\infty} \sigma(E)dE/E^{1+\alpha} \qquad 2.34$$

The relation between I_0 and $I_0(\alpha)$ necessitates the introduction of the so-called effective resonance energy $\bar{E}_r$.

The direct experimental determination of the epicadmium reaction rate, R_e is possible when a nuclide is irradiated under a Cd-cover in the afore-mentioned standard conditions, R_e is simply described by:

$R_e = \phi_e I_0 (\alpha)$ (or $R_e = \phi_e I_0$) 2.35

The sub-cadmium reaction rate, R_s is then the difference between the experimentally determined R and R_e values. R_s is described by:

$R_s = \phi_s \sigma_0$ 2.36

Another useful quantity is the experimentally determined Cd – ratio, R_{cd}:

$$R_{cd} = \frac{R}{R_e} = \frac{\phi_s \sigma_0 + \phi_e I_0(\alpha)}{\phi_e I_0(\alpha)} = \frac{f}{Q_0(\alpha)} + 1 \qquad 2.37$$

$$\text{or } R_{cd} = \frac{\phi_s \sigma_0 + \phi_e I_0}{\phi_e I_0} = \frac{f}{Q_0} + 1 \qquad 2.38$$

where $f = \phi_s/\phi_e$ is the ratio of sub cadmium to epithermal flux,

$Q_0 (\alpha) = I_0 (\alpha)/\sigma$ and $Q_0 = I_0/\sigma$ 2.39

It is important to note that R and R_e cannot be measured simultaneously by irradiating together a bare and Cd- covered nuclide, since Cd causes significant flux depressions in its vicinity (IAEA, 1970).

2.3.1 The Hϕgdahl's Convention

This convention is the most practical for activation analysis and its mechanism is as follows:

i. Firstly, σ_0 and I_0 values are found for an ultimate cross section standard by methods independent of neutron activation (Holden, 1981). The most common standard is ^{197}Au (n, γ) ^{198}Au, with the following recommended

data, adopted in this work: σ_0= 98.65±0.09barn (±0.09%), I_0 = 1550 ± 28 barns (± 1.8%) and Q_0 = 15.71 ± 0.28 (1.8%) (De Corte, 1987).

ii. Then, by measuring R_{Au} and $R_{e,\,Au}$, one can determine ϕ_s, ϕ_e and f, for any irradiation site from Eqs. 2.35, 2.36 and 2.37 respectively, if $I_{0,\,Au}$ has been converted to $I_{0,\,Au}$ (α).

iii. Finally, applying the same equations, one can determine σ_0, I_0 and Q_0 from R and R_e measurement for other (n,γ) reactions after converting I_0 (α) to I_0.

2.3.2 Neutron Self Shielding and Cd – transmission Factors

It is necessary to introduce some correction factors in the equations describing R and R_e in order to link the reaction rate to the signal obtained from (n,γ) activation. These correction factors are:

i. The thermal neutron self-shielding factors (G_{th}≤1). This is a correction term that depends on the nucleus density and on σ_0. G_{th} has to be multiplied by $\phi_s\sigma_0$ in order to obtain the observed reaction rates for actual samples. Historically, this has been interpreted in terms of the average thermal flux ($\phi_s = G_{th}\,\phi_s$) inside the sample

ii. Epithermal neutrons self-shielding factor ($G_e \leq 1$), this also depends on the nucleus density and resonance parameters. Thus to be multiplied by $\phi_e I_0$ (α) [or $\phi_e I_0$] in order to obtain the observed reaction rates for actual samples. Historically, this has been interpreted in terms of the effective resonance integral I_{eff} (α) = G_e I_0 (α) of a material which is not diluted.

iii. For most nuclides, the Cd-transmission factor for epithermal neutrons (F_{cd}), is equal to unity. For some others, it is less than one and in exceptional cases, it can be greater than one. It has to be multiplied by $\phi_e I_0(\alpha)$ [or $\phi_e I_0$], but only when an irradiation is done under Cd – cover.

In view of the above, Eqs. 2.33, 2.34, 2.35 and 2.37 should be written as

$$R = G_{th}\phi_s\sigma_0 + G_e\phi_e I_0(\alpha) \qquad 2.40$$

$$R_e = G_e F_{cd}\phi_e I_0(\alpha) \qquad 2.41$$

$$R_s = G_{th}\phi_s\sigma_0 \ (only\ if\ F_{cd} = 1) \qquad 2.42$$

$$F_{cd}R_{cd} = \left[\frac{G_{th}f}{G_e Q_0(\alpha)}\right] + 1 \qquad 2.43$$

and similarly for $\alpha = 0$

2.3.3 The Activation Equation

By considering the (n,γ) activation with subsequent gamma-spectrometry, it could be shown that the relation between the reaction rate and the number of counts (N_p) collected in the full-energy peak is given by:

$$R = \frac{N_p/t_m}{\frac{SDCw}{N_A\theta\varepsilon_p\gamma/M}} \qquad 2.44$$

or

$$R = \left(\frac{N_p/t_m}{SDCw}\right)_{cd} / \frac{N_A\theta\varepsilon_p\gamma}{M} \qquad 2.45$$

on condition that the measured radionuclide is directly formed by (n,γ) and that disappearance of target and formed nuclei by (n,γ) reaction is negligible (i.e. no burn up effects).

Where:

N_p = number of counts in the full- energy peak

t_m = measuring time (s)

S = Saturation factor $(1-e^{-\lambda t_{irr}})$; λ is the decay constant (λ = ln2/$T_{1/2}$), with $T_{1/2}$ being the half-life, t_{irr} is the irradiation time.

D = decay factor ($e^{-\lambda t_d}$); t_d is decay time (s).

C = measurement factor ($(1-e^{-\lambda t_m})/\lambda t_m$); t_m is the measurement time.

w = mass of irradiated element in (g)

θ = Isotopic abundance (fraction)

ε_p = full energy peak detection efficiency

γ = Absolute gamma intensity.

M = Atomic weight

Now, let the specific count rate ($s^{-1}g^{-1}$) be denoted by:

$$A_{sp} = \frac{N_p / t_m}{SDCw} \qquad 2.46$$

Then, by substituting eq. 2.46, 2.40 and 2.41 in eq. 2.44 and 2.45, we obtain the activation equation.

$$A_{sp} = \frac{N_A \theta \gamma}{M}\left[G_{th}\phi_s\sigma_0 + G_e\phi_e I_0(\alpha)\right]\varepsilon_p \qquad 2.47$$

or

$$(A_{sp})_{cd} = \frac{N_A \theta \gamma}{M} G_e F_{Cd}\phi_s I_0(\alpha)\varepsilon_p \qquad 2.48$$

The difference between eqs. 2.47 and 2.48 is called the Cd – difference, provided the same ε_p – value is involved. One has:

$$A_{sp} - (A_{sp})_{cd} / F_{cd} = \frac{N_A \theta \gamma}{M} G_{th} \phi_s \sigma_0 \varepsilon_p \qquad 2.49$$

Hence, the experimentally measured Cd – ratio, R_{cd}, is simply obtained as

$$R_{cd} = \frac{A_{sp}}{(A_{sp})_{cd}} \qquad 2.50$$

2.3.4 Principles of Standardization

Provided the neutron irradiation facility is kept unchanged, the neutron flux will be constant and hence, the induced activity will only be a function of irradiation, measuring and decay time. Therefore, in cases of irradiation, only the source strength as a function of time will have to be taken into account, as the decay time of source is well known. Consequently the system needs to be standardized only once.

In (n,γ) activation analysis, the mass of the element to be determined (i.e. the analyte, index a) in the sample can be obtained from eq. 2.47 and 2.48, when the sample is irradiated in the whole neutron spectrum (NAA) and under cadmium cover (ENAA) yielding respectively:

$$W_a = \frac{M_a}{N_A \theta_a \gamma_a} \frac{\left(\frac{N_p / t_m}{SDC} \right)_a}{(G_{th,a} \phi_s \sigma_{0,a} + G_{e,a} \phi_e I_{0,a}(\alpha) \varepsilon_{p,a}} \qquad 2.51$$

$$W_a = \frac{M_a}{N_A \theta_a \gamma_a} \frac{\left[\left(\frac{N_p / t_m}{SDC} \right)_{cd} \right]_a}{G_{e,a} F_{cd,a} \phi_e I_{0,a}(\alpha) \varepsilon_{p,a}} \qquad 2.52$$

The actual determination of W_a can be based on various standardization methods:

2.3.5 Relative Standardization

In this method, each sample is co-irradiated with a known mass of the element (standard, index, s) to be determined; both are later counted in the same geometry with respect to the detector. Thus eqs. 2.51 and 2.52 could be written as:

$$W_a = \frac{\left(\frac{N_p / t_m}{DC}\right)_a}{\left(\frac{N_p / t_m}{DCw}\right)_s} \bullet \frac{G_{th,s} f + G_{e,s} Q_{0,s}(\alpha)}{G_{th,a} f + G_{e,a} Q_{0,a}(\alpha)} \bullet \frac{\varepsilon_{p,s}}{\varepsilon_{p,a}} \qquad 2.53$$

and

$$W_a = \frac{\left(\frac{N_p / t_m}{DC}\right)_{cd,a}}{\left(\frac{N_p / t_m}{DCw}\right)_{cd,s}} \bullet \frac{G_{e,s}}{G_{e,a}} \bullet \frac{\varepsilon_{p,s}}{\varepsilon_{p,a}} \qquad 2.54$$

respectively, since $S_a = S_s$, $M_a = M_s$, $\gamma_a = \gamma_s$, $\sigma_{o,a} = \sigma_{o,s}$, $I_{o,a} = I_{o,s}$ and $\theta_a = \theta_s$

In the above, it has been assumed that flux gradients between sample and standard location in the irradiation container are negligible or corrected for. The f-factor can be eliminated only if:

$G_{e,s}Q_{0,s}(\alpha) \ll G_{th,s}f$ and $G_{e,a}Q_{0,a}(\alpha) \ll G_{th,a}f$;

or $G_{th,s} = G_{th,a} = G_{e,s} = G_{e,a} = 1$. Then, eqs. 2.54 and 2.55 may be written as:

$$W_a = \frac{\left(\frac{N_p / t_m}{DC}\right)_a}{\left(\frac{N_p / t_m}{DCw}\right)_s} \qquad 2.55$$

and

$$W_a = \frac{\left[\left(\frac{N_p / t_m}{DC}\right)_{cd}\right]_a}{\left[\left(\frac{N_p / t_m}{DCw}\right)_{cd}\right]_s} \qquad 2.56$$

for NAA and ENAA respectively.

In terms of concentration, they are given by:

$$\rho_a(ppm) = \frac{\left(\frac{N_p / t_m}{DCw}\right)_a}{\left(\frac{N_p / t_m}{DCw}\right)_s} \times 10^6 \qquad 2.57$$

and

$$\rho_a(ppm) = \frac{\left[\left(\frac{N_p / t_m}{DCw}\right)_a\right]_{cd}}{\left[\left(\frac{N_p / t_m}{DCw}\right)_s\right]_{cd}} \times 10^6 \qquad 2.58$$

respectively, where w is the sample mass in grams.

This method is the most prevalent in NAA. It can be performed with individual mono element standards or natural multi-element standards. It is assumed that in favorable conditions, its accuracy is about 1 to 2% (De Corte, 1987). However, the obvious disadvantage of the method in routine multi element NAA, where sample preparation, counting and spectra evaluation of the standards is laborious and irksome, especially in the case of unexpected elements for which no standard has been co irradiated. To prevent some of these problems, it is recommended that one uses: (i) home made reference materials (ii) commercially multi elements reference materials (e.g. USGS/, United States Geological Survey), standard reference materials (e.g., SRM1), National Bureau of Standards, certified reference materials (e.g. BCR-CRM1, Community Bureau of reference), and the like. It should be remarked here that in view of the limited quantities available, their use for standardization on routine basis is not justifiable; moreover, their accuracies quoted on the specified elemental concentrations are even in the best cases not better than 5%. It should be noted that in this type of standardization, greatest similarity between sample and standard should be aimed at.

2.3.6 The Absolute Method

If eq. 2.47 is expressed for the analyte and a flux monitor (index, m) co-irradiated with the sample, the combination leads to,

$$\rho_a(ppm) = \frac{\left(\frac{N_p/t_m}{SDCw}\right)_a}{A_{sp,m}} \bullet \frac{M_a\theta_m\gamma_m\sigma_{0,m}}{M_m\theta_a\gamma_a\sigma_{0,a}} \bullet \frac{G_{th,m}f + G_{e,m}Q_{0,m}(\alpha)}{G_{th,a}f + G_{e,a}Q_{0,a}(\alpha)} \bullet \frac{\varepsilon_{p,m}}{\varepsilon_{p,a}} \times 10^6 \qquad 2.59$$

assuming that ϕ_s, f and α remain constant during irradiation.

This method, though experimentally very simple, requires the accurate knowledge of the parameters, M,θ, γ and σ_o for both analyte and monitor, which may lead to the loss of accuracy and tractability of the analytical results. Since σ_o, γ and θ can be sources of considerable errors or uncertainties.

2.3.7 The Single Comparator Method

Girardi originated this technique (De Corte, 1987). In its original form, the NAA single Comparator method utilizes the so-called k-factors, which are experimentally determined by co irradiation of a standard and a single comparator (monostandard, index c)

$$k_c(s) = \frac{A_{sp,s}}{A_{sp,c}} \qquad 2.60$$

From eq. 2.47, it implies that the definition of $k_c(s)$ is:

$$k_c(s) = \frac{M_c\theta_s\gamma_s\sigma_{0,s}}{M_s\theta_c\gamma_c\sigma_{0,c}} \bullet \frac{G_{th,s}f + G_{e,s}Q_{0,s}(\alpha)}{G_{th,c}f + G_{e,c}Q_{0,c}(\alpha)} \bullet \frac{\varepsilon_{p,s}}{\varepsilon_{p,c}} \qquad 2.61$$

It follows that the concentrations of the analyte can be obtained from co irradiation of sample and single comparator.

$$\rho_a, ppm = \frac{\left(\frac{N_p / t_m}{SDCw}\right)_a}{A_{sp,c}} \bullet \frac{1}{k_c(s)} \bullet 10^6 \qquad 2.62$$

provided that $\theta_a = \theta_s$ $G_{th} = G_e = 1$, f and α show no significant difference in the irradiation conditions of analysis and $k_c(s)$ determination, the detection efficiency is the same for analyte/comparator and standard/ comparator in the counting conditions of analysis and $k_c(s)$ – determination, all flux parameters (ϕ_s, f and α) remain constant during irradiation, for both analysis and $k_c(s)$ determination.

When properly performed, it has an estimated accuracy of 3% or less. Its' obvious advantage is the experimental simplicity, on condition that k-factors are determined a priori. It is useful in routine analysis of long series of similar samples (De Corte, 1987).

The draw back of the method is the rigidity of the k-factors which are strictly bound to local and "personal" experimental conditions, sometimes with awkward consequence.

2.3.8 The k_o- Standardization

In the k_0 standardization of NAA, the concentration of the analyte 'a' is obtained from its measured isotope/gamma ray as

$$\rho_a = \frac{\left(N_P / Wt_m SDC\right)_a}{\left(N_P / wt_m SDC\right)_{Au}} x \frac{1}{k_{0,Au}(a)} x \frac{f + Q_{0,Au}(\alpha)}{f + Q_{0,a}(\alpha)} x \frac{\varepsilon_{P,Au}}{\varepsilon_{P,a}} \qquad 2.63$$

where 'Au' refers to the co-irradiated gold monitor [^{197}Au (n,() ^{198}Au, $E_($=411.8 keV] and

N_p = the number of counts in the full energy peak.

w = weight of the gold monitor

W = weight of the sample

S = $(1 - e^{-\lambda tirr})$, saturation factor

D = $e^{-\lambda td}$, Decay factor

C = $(1 - e^{-\lambda tm})$ Counting factor

t_d = decay time

t_{ur} = irradiation time

t_m = measuring time

λ = Decay constant

f = thermal to epithermal neutron flux ratio

$Q_{o,}$ = I_o/σ_o is the ratio of resonance integral to thermal neutron capture cross section at neutron velocity of 2200 ms^{-1}.

α = epithermal neutron flux distribution, approximated by a $1/ E^{1+\forall}$ dependence (with α considered to be independent of neutron energy)

ε_P = the full energy peak detection efficiency.

Furthermore, in Eq. 2.63, the $k_{0,Aa}(a)$ factor is defined as

$$k_{0,Au}(a) = \frac{M_{Au}\,\theta_a\,\sigma_{0,a}\,\gamma_a}{M_a\,\theta_{Au}\,\sigma_{0,Au}\,\gamma_{Au}} \qquad 2.64$$

where M is the atomic weight, θ is the isotopic abundance, σ_0 is the 2200 m/s (n,γ) cross section, and γ is the absolute gamma ray intensity (emission probability).

Although the k_0 factors are defined versus Au (co-irradiated with the sample to be analyzed), the gold monitor can be replaced by any monitor 'm' for which a $k_{0,Au}(a)$ factor is available, because

$$k_{0,m}(a) = k_{0,Au}(a) \,/\, k_{0,Au}(m) \qquad 2.65$$

Eq. 2.63 is written in the Hogdahl formalism (modified for a 1/ $E^{1+\alpha}$ epithermal flux shape for which it is required that the cross section in the thermal neutron region varies as 1/*v*. whereas this requirement is fulfilled to a good approximation by most analytically interesting (n, γ) reactions, there are some exceptions where the deviation is significant. In these cases, the Wescott formalism, with the introduction of the epithermal shape factor, is applicable, and the

$[f + Q_{0,Au}(\alpha)] / [f + Q_{0,a}(\alpha)]$ ratio in Eq. 2.63 should be replaced by

$$\frac{g_{Au}(T_n) + r(\alpha)\sqrt{T_n / T_0}\ x\ s_{0,Au}(\alpha)}{g_a(T_n) + r(\alpha)\sqrt{T_n / T_0}\ x\ s_{0,a}(\alpha)} \qquad 2.66$$

where $g(T_n)$ is the 'Wescott's g-factor depending on the neutron temperature T_n, which is a measure of the deviation from the 1/*v* cross section behavior, $r(\alpha)\ \sqrt{(T_n/T_o)}$ is the spectral index (modified for $1/E^{1+\alpha}$ epithermal spectrum), with T_n being the actual Maxwellian neutron temperature, and T_0 =293.6K, and $s_0(\alpha)$ is a measure for the epithermal to thermal (n,γ) cross section (modified for a $1/E^{1+\alpha}$ epithermal spectrum).

For a 1/*v* thermal cross section behavior, one has, to a good approximation

$$s_0 = \frac{2}{\sqrt{\pi}} Q_0 - 0.484 \qquad 2.67$$

The conversions from the Q_0 values to $Q_0(\alpha)$ and from s_0 values to $s_0(\alpha)$, is given by

$$Q_0(\alpha) = \left[\frac{Q_0 - 0.429}{(\overline{E}_r)^{\alpha}} + \frac{0.429}{(2\alpha + 1)(E_{Cd})^{\alpha}} \right] (1\ eV)^{\alpha} \qquad 2.68$$

and

$$s_0(\alpha) = s_0(\overline{E}_r)^{-\alpha} (1\ eV)^{\alpha} \qquad 2.69$$

where E_{Cd} is the effective Cd cut-off energy (=0.55eV in standard conditions) and $\overline{E}_r$ is the effective resonance energy. The $(1\ eV)^{\forall}$ term (numerically unity) originates from the

definition of the epithermal neutron flux in a $1/E^{1+\alpha}$ distribution. The above treatise holds for the case where the analytical isotope is directly formed by (n, γ) reaction.

The k_0 factors are experimentally measured (in Hogdahl formalism) according to the equation

$$k_{0,Au} = \frac{(N_P / wt_m SDC)_a}{(N_P / wt_m SDC)_{Au}} x \frac{f + Q_{0,Au}(\alpha)}{f + Q_{0,a}(\alpha)} x \frac{\varepsilon_{P,Au}}{\varepsilon_{P,a}} \qquad 2.70$$

where w is the mass of the element under consideration and $k_{0,Au}$ is written for short instead of $k_{0,Au}(a)$. An alternative technique makes use of the 'Cd-subtraction method' in which

$$k_{0,Au} = \frac{\left[(N_P / wt_m SDC) - (N_P / wt_m SDC)_{Cd} / F_{Cd}\right]_a}{\left[(N_P / wt_m SDC) - (N_P / wt_m SDC)_{Cd} / F_{Cd}\right]_{Au}} x \frac{\varepsilon_{P,Au}}{\varepsilon_{P,a}} \qquad 2.71$$

where 'Cd' refers to irradiation of the materials under cadmium cover and F_{Cd} is the cadmium transmission factor for epithermal neutrons (usually=1, but $F_{Cd,Au} = 0.991$).

As to the measurement of Q_0 values, the well-known cadmium ratio method (in the Hogdahl formalism) is used, and

$$Q_0(\alpha) = \frac{f}{F_{Cd} R_{Cd} - 1} \qquad 2.72$$

followed by conversion of Q_0 (α) to Q_0 according to Eq. 2.68. Similarly, in the Wescott formalism

$$s_0(\alpha) = \{g(T_n) / (F_{Cd} R_{Cd} - 1)\} / \left\{ \frac{g(T_n)(1eV)^\alpha}{K(1+2\alpha)(E_{Cd})^\alpha} - W'(\alpha) \frac{2}{\sqrt{\pi}} \right\} \qquad 2.73$$

where $R_{Cd} = \frac{(N_P / wt_m SDC)}{(N_P / wt_m SDC)_{Cd}}$, the cadmium ratio, K = 0.25 $(BE_{Cd} / E_0)^{1/2}$, with E_0 = 0.0253 eV, and $W'(\alpha) = W'(\overline{E_r})^{-\alpha} (1\ eV)^\alpha$, with W' a small correction term for a non-1/*v*

cross section behavior between kT_n (equivalent cutoff value of the epithermal neutron flux) and E_{Cd}. The conversion of s_0 (α) to s_0 is then performed according to Eq. 2.69.

The effective resonance energy $\overline{E}_r$ is defined as

$$(\overline{E}_r)^{-\alpha} = \frac{I_0'(\alpha)}{I_0'}(1eV)^{-\alpha} \qquad 2.74$$

where I'_0 and I_0 (α) are the reduced resonance integrals ($1/v$ tail subtracted) for 1/E and a $1/E^{1+\alpha}$ epithermal neutron flux distribution, respectively. Although $\overline{E}_r$ is primarily a function of α, it can to a good approximation be calculated as an α-independent value, according to

$$\ln \overline{E}_r = \frac{\sum_i w_i \ln E_{r,i}}{\sum_i w_i} \qquad 2.75$$

where the weighting factor w_i is given by

$$w_i = \left(\frac{g\Gamma_\gamma \Gamma_n}{\Gamma}\right)_i \frac{1}{E_{r,i}^2} \qquad 2.76$$

where g is the statistical weight factor, Γ_γ is the radiative width, Γ_n is the neutron width, and Γ is the total width of resonance.

2.4 Determination of f and α - Values

Despite many attempts to describe α - theoretically, its experimental determination has remained as the only reliable means of obtaining its value (Jovanovic *et al*., 1989). In principle, there are three experimental methods of α- determination namely: Cd-covered method, Cd-ratio method and bare method. Of the three, the Cd- ratio multi-monitor method is the most accurate (Jovanovic et *al*., 1989) and is the one used in this work.

In the "Cd-ratio for multi-monitor" method for the determination of *f* and α (measure of the deviation of epithermal neutrons from the ideal 1/E distribution), the parameters are defined

as $$f = Q_{0,i}.(\alpha).(F_{Cd,i}.R_{Cd,r} - 1).\frac{G_{e,i}}{G_{th,i}} \qquad 2.77$$

where i is the monitor with well known Q_o-value.

If a set of N monitors is irradiated with and without Cd cover, and the induced activities are measured with a detector, with all the monitors obeying the σ(ν) versus 1/ν dependence, α is the slope of the straight line plot of

$$\log \frac{\overline{E}_{r,i}^{\alpha}}{(F_{Cd.}R_{Cd,i} - 1)Q_{0,i}(\alpha)G_{e,i}/G_{th,i}} \quad \text{versus} \quad \log E_{r,i} \qquad 2.78$$

Mathematically, by using an iterative procedure for a set of N monitors, equation 2.78 can be rewritten as equation 2.79 below and the α-value is found as the root of the equation.

$$\alpha + \frac{\sum_{i=1}^{N}\left[\left(\log\overline{E}_{r,i} - \frac{\sum_{i=1}^{N}\log\overline{E}_{r,i}}{N}\right)\left(\log\frac{E_{r,i}^{\alpha}}{(F_{Cd,i}R_{Cd,i}-1)Q_{0,i}(\alpha)G_{e,i}/G_{th,i}} - \frac{\sum_{i=1}^{N}\log\frac{E_{r,i}^{\alpha}}{(F_{Cd,i}R_{Cd,i}-1)Q_{0,i}(\alpha)G_{e,i}/G_{th,i}}}{N}\right)\right]}{\sum_{i=1}^{N}\left(\log\overline{E}_{r,i} - \frac{\sum_{i=1}^{N}\log\overline{E}_{r,i}}{N}\right)^2} = 0 \qquad 2.79$$

where, $$R_{Cd} = \frac{A_{sp.bare}}{A_{sp.Cd}} \qquad 2.80$$

$$A_{sp} = \left[\frac{N_p/t_m}{wSDC}\right] \qquad 2.81$$

i. denotes the i^{th} monitor, and N, the number of monitors used

$E_{r,i}$ is the effective resonance energy of the i^{th} monitor

F_{cd} is the Cd-transmission factor for epithermal neutrons

G_{ei} is the epithermal neutron self-shielding factor for the i^{th} monitor.

$G_{th,i}$ is the thermal neutron self-shielding factor for the i^{th} monitor

$R_{cd,i}$ is the ratio of the specific activity of the i^{th} monitor irradiated without Cd ($A_{sp.bare}$) to that with Cd cover (A_{spCd}).

$Q_{o,i} = I_o/\sigma_o$ is the ratio of resonance integral to thermal neutron capture cross section at neutron velocity of 2200 m/s for the i^{th} monitor.

2.5 Monitoring of specific flux parameters

In terms of the modified Westcott's formalism, the equation for elemental concentration calculation according to the k_0-method is:

$$\rho = \frac{\frac{N_p / t_m}{SDCW}}{\left(\frac{N_p / t_m}{SDCw}\right)^*} \cdot \frac{1}{k_0} \cdot \frac{g^*(T_n) + r(\alpha)\sqrt{T_n / T_0}\,.\,s_0^*(\alpha)}{g\,(T_n) + r(\alpha)\sqrt{T_n / T_0}\,.\,s_0(\alpha)} \cdot \frac{\varepsilon_p^*}{\varepsilon_p} \qquad 2.82$$

where * stands for co-irradiated monitor, W is the sample mass, w is the monitor mass and $g(T_n)$ is the Westcott's factor which enables one to correct for a "non-1/v" behaviour. From Eq. 2.82, the flux parameters to be monitored are α, $r(\alpha)\sqrt{(T_n/T_0)}$ and T_n. Analogous to the solution given in terms of the Hogdahl convention, α can be determined from the slope (-α) of the straight line when plotting log T_i versus $\log(\overline{E}_{r,i}/1eV)$, which comes to the same as solving the implicit equation

$$\alpha + \frac{\sum_{i=1}^{N}\left\{\left[\log \overline{E}_{r,i} - \sum_{i=1}^{N}\frac{\log \overline{E}_{r,i}}{N}\right]\left[\log T_i - \sum_{i=1}^{N}\frac{\log T_i}{N}\right]\right\}}{\sum_{i=1}^{N}\left[\log \overline{E}_{r,i} - \sum_{i=1}^{N}\frac{\log \overline{E}_{r,i}}{N}\right]^2} = 0 \qquad 2.83$$

where N is the number of co-irradiated α-monitors, and T_i is given by the expression

i) In the "Cd-ratio for multi-monitor" method:

$$T_i = \frac{G_{th,i} \cdot g_i(T_n) \cdot (1eV)^{\alpha} \cdot (\overline{E}_{r,i})^{-\alpha}}{R_{Cd,i} \cdot F_{Cd,i} \left[\frac{g_i(T_n) \cdot (1eV)^{\alpha}}{K(1+2\alpha) E_{Cd}^{\alpha}} - \frac{2}{\sqrt{\pi}} W_i'(\alpha) + G_{r,i} \cdot s_{0,i}(\alpha) \right] - G_{r,i} \cdot s_{0,i}(\alpha)} \qquad 2.84$$

ii) In the "Cd-covered multi-monitor" method:

$$T_i = \frac{\frac{\left(\frac{N_p / t_m}{SDCw} \right)_{epiCd}}{k_{0,Au}(i) \varepsilon_{p,i}} (1eV)^{\alpha} (\overline{E}_{r,i})^{-\alpha} (1\, gs)}{F_{Cd,i} \left[\frac{g_i(T_n)(1eV)^{\alpha}}{K(1+2\alpha) E_{Cd}^{\alpha}} - \frac{2}{\sqrt{\pi}} W_i'(\alpha) + G_{r,i} \cdot s_{0,i}(\alpha) \right]} \qquad 2.85$$

iii) In the "bare multi-monitor" method:

$$T_i = \frac{\left[G_{th,ref} \frac{k_{0,Au}(ref)}{k_{0,Au}(i)} \cdot \frac{\varepsilon_{p,ref}}{\varepsilon_{p,i}} g_{ref}(T_n) - G_{th,i} \frac{A_{sp,ref}}{A_{sp,i}} \cdot g_i(T_n) \right] (1eV)^{\alpha} (\overline{E}_{r,i})^{-\alpha}}{G_{r,i} \frac{A_{sp,ref}}{A_{sp,i}} \cdot s_{0,i}(\alpha) - G_{r,ref} \frac{k_{0,Au}(ref)}{k_{0,Au}(i)} \cdot \frac{\varepsilon_{p,ref}}{\varepsilon_{p,i}} s_{0,ref}(\alpha)} \qquad 2.86$$

with "ref" representing a co-irradiated reference monitor.

In the above, preferably, use is made of "1/v" monitors, so that $g(T_n) = 1$, otherwise an iterative procedure has to be followed.

The modified spectral index, which is a measure for the epithermal to total neutron density ratio, can be obtained from the Cd-ratio method for a suitable monitor by:

$$r(\alpha) \sqrt{T_n / T_0} = \frac{G_{th} \cdot g(T_n)}{R_{Cd} \cdot F_{Cd} \left[\frac{g(T_n) \cdot (1eV)^{\alpha}}{K(1+2\alpha) E_{Cd}^{\alpha}} - \frac{2}{\sqrt{\pi}} W'(\alpha) + G_r \cdot s_0(\alpha) \right] - G_r \cdot s_0(\alpha)} \qquad 2.87$$

or from the "bare dual monitor"- method:

$$r(\alpha)\sqrt{T_n/T_0}=\frac{\left[\frac{k_{0,Au}(1)}{k_{0,Au}(i)}.\frac{\varepsilon_{p,1}}{\varepsilon_{p,i}}g_1(T_n)-\frac{A_{sp,1}}{A_{sp,2}}.g_2(T_n)\right]}{\frac{A_{sp,1}}{A_{sp,2}}.s_{0,2}(\alpha)-\frac{k_{0,Au}(1)}{k_{0,Au}(2)}.\frac{\varepsilon_{p,1}}{\varepsilon_{p,2}}s_{0,1}(\alpha)} \qquad 2.88$$

Here again it is advised to use "1/v" monitors with $g(T_n) = 1$.

Finally, T_n is determined by co-irradiating Lu with a "1/v" [$g(T_n) = 1$] monitor and

$$g_{Lu}(T_n)=\left[\frac{\frac{A_{sp,Lu}/G_{th,Lu}}{k_{0,Au}(Lu)\,\varepsilon_{p,Lu}}}{\frac{A_{sp,1/v}}{k_{0,Au}(1/v)\varepsilon_{p,1/v}}}\right]\left[G_{th,1/v}.g_{1/v}(T_n)+G_{r,1/v}.r(\alpha)\sqrt{T_n/T_0}.s_{0,1/v}(\alpha)\right] - \frac{G_{r,Lu}}{G_{th,Lu}}.r(\alpha)\sqrt{T_n/T_0}.s_{0,Lu}(\alpha) \qquad 2.89$$

Eq. 2.89 yields $g_{Lu}(T_n)$ and from tables of $g_{Lu}(T_n)$ versus T_n, finally T_n is obtained.

CHAPTER THREE

MATERIALS AND METHODS

3.1 Materials

The materials required for this work include:-

- Standard γ-ray sources.
- HPGe Gamma-ray spectrometer
- Neutron monitor foils.
- NIRR-1
- Nuclides whose reactions cross sections are to be determined

3.1.1 Standard sources

These are the standard γ-ray sources whose activities and date of manufacture are known. They were used to perform both energy and efficiency calibration of the HPGe detector. The sources used are:- ^{22}Na, ^{54}Mn, ^{57}Co, ^{60}Co, ^{137}Cs, ^{152}Eu, ^{226}Ra and ^{241}Am.

Table 3.1 Nuclear data of standard gamma sources

Radionuclide	Half-life	Activity (kBq)	Date of manufacture
^{241}Am	432.2 y	36.5	01-07-04
^{226}Ra	1600 y	37.4	,,
^{152}Eu	13.5 y	38.0	15-07-04
^{137}Cs	30.18 y	36.9	,,
^{88}Y	106.6 d	35.8	,,
^{60}Co	5.271 y	38.4	,,
^{57}Co	271.73 d	37.7	,,
^{54}Mn	312.2 d	38.7	,,
^{22}Na	2.604 y	36.9	,,

*produced by Damri, Cedex, France.

3.1.2 Monitor foils

The monitor foils that were used for the characterization i.e. the determination of the neutron spectrum parameters of the irradiation sites are high purity foils and alloys of Lu, Zn, Zr and Au. Their description is as given in Table 3.2.

Table 3.2 Description of the monitor foils used.

Monitor	Material description	Diameter, cm	Range of mass, mg
Au	Al-0.1% Au; 0.1mm thick, IRMM-530	0.8	12-14
Zn	99.95% Zn foil, 0.025mm thick Goodfellow.	0.8	4-5
Zr	99.8% Zr foil; 0.125 mm thick, Goodfellow	0.8	44-46
Lu	Al -0.1% Lu 0.1mm thick, IRMM	0.5	2-3

3.13 Reaction Cross Section Determination

These are the neutron-induced nuclear reactions whose activation cross sections and or resonance integrals were measured. The thermal cross sections σ_0; resonance integrals, I_0, or the ratio of resonance integrals to thermal cross sections Q_0, from references, show large differences of between 5-20%. These nuclides include:- ^{72}Ga; ^{110m}Ag; ^{56}Mn; ^{95}Zr; ^{97}Zr; ^{239}U; ^{75}Se; ^{76}As; ^{49}Ca.

The description of the monitors and the nuclear data of reactions to be measured or reevaluated are as given in Tables 3.3a and 3.3b.

Table 3.3a Description of monitor foils and oxides used.

Target	Material description	Diameter, cm	Range of mass, mg
Au	Al-0.1% Au; 0.1mm thick, IRMM-530	0.8	12-14
Mn	Mn-1% Al foil, 0.1mm thick, SP89070 IRMM.	0.6	3-5
Zr	99.8% Zr foil; 1mm thick, Goodfellow	0.6	42-45
U	U-0.2% Al foil, 0.1mm thick, NS2017 IRMM.	0.6	43-53
Se	SeO_2 powder, Merck KGaA	-	51-63
Ag	Ag_2O powder, Merck KGaA	-	50-51
Ga	Ga_2O_3 powder, Riedel-de-Haën.	-	52-62
Ca	CaO powder, Merck KGaA	-	54-57
As	As_2O_3 powder, Riedel-de-Haën.	-	52-54

Table 3.3b. Nuclear data of monitor foils and oxides used.

Atomic Weight	Target	product	$T_{½}$	E_r	θ,%	E_γ, keV	γ, %
74.92	^{75}As	^{76}As	26.32h	106	100	559.1	44.6
						559.2	46.2
						563.2	1.6
						657.1	6.4
						1212.9	1.8
						1212.9 + 1216.1	5.5
						1216.1	3.7
196.97	^{197}Au	^{198}Au	2.695d	5.65	100	411.8	95.53
54.94	^{55}Mn	^{56}Mn	2.579h	468	100	846.8	99
						1810.7	27.2
						2113.1	14.3
91.22	^{95}Zr	^{96}Zr	34.97d	6260	17.28	765.8	99
238.03	^{238}U	^{239}U	23.45m	16.9	99.2746	74.7	
78.96	^{74}Se	^{75}Se	119.8d	29.4	0.9	121.1	16.41
						136	56.02
						264.7	58.6
						279.5	24.73
						400.7	11.13
107.87	^{109}Ag	^{110m}Ag	249.76d	6.08	48.17	446.8	3.657
						620.4	2.776
						657.8	94.74
						677.6	10.8621
						687	6.49
						706.7	17.0242
						744.3	4.661
						763.9	22.36
						818	7.323
						884.7	72.86
						937.5	34.31
						1384.3	24.35
						1475.8	3.989
						1505	13.11
						1562.3	1.184
69.72	^{71}Ga	^{72}Ga	14.1h	154	39.9	630	24.37
						834	99.55
						894.2	9.842
						1050.7	6.921
						2201.7	26.06
						2491	7.472
						2501.8	20.52
						2507.9	13.05
40.08	^{48}Ca	^{49}Ca	8.718m	1330000	0.187	3084.4	91.7

3.14 The Nigeria Research Reactor-1 (NIRR-)

The NIRR1 has a tank-in-pool structural configuration with a nominal power rating of 31kW. It has a built-in clean cold core excess reactivity of 3.77mk and can operate for a maximum of 4.5 hours at full power (i.e. equivalent to a thermal neutron flux of $1x10^{12}$ n cm^2 s^{-1} in the inner radiation channels). Under these conditions, the reactor can operate with the same fuel loading for over ten years with a burn-up of <1%. (Jonah et al., 2005).

The NIRR1 consists of five small inner rabbit tubes, which are installed inside the beryllium annulus. Between the beryllium annulus and the reactor vessel, three small and two large rabbit tubes are installed. They are designed as the outer irradiation channels. Out of a total of ten irradiation channels of NIRR1, six are connected to the pneumatic transfer systems. There are two sets of transfer systems; the pneumatic transfer system type A, which is connected to two of the irradiation channels, A_1, (small, inner channel) and A_2 (large, outer channel) is suitable for handling middle and long-lived nuclides. The other is a multi-functional transfer system, the pneumatic transfer system B. This is connected to three small inner irradiation channels (B_1, B_2 & B_3) and a small outer irradiation channel B_4. System B can be used to send a sample into the reactor and retrieve it to a specified position such as detector, stripper or waste tank. It is especially designed for NAA of short-lived nuclides and is suitable for cyclic NAA of nuclides with half-lives in seconds. The core configuration of the NIRR-1 is shown in Figure 3.1.

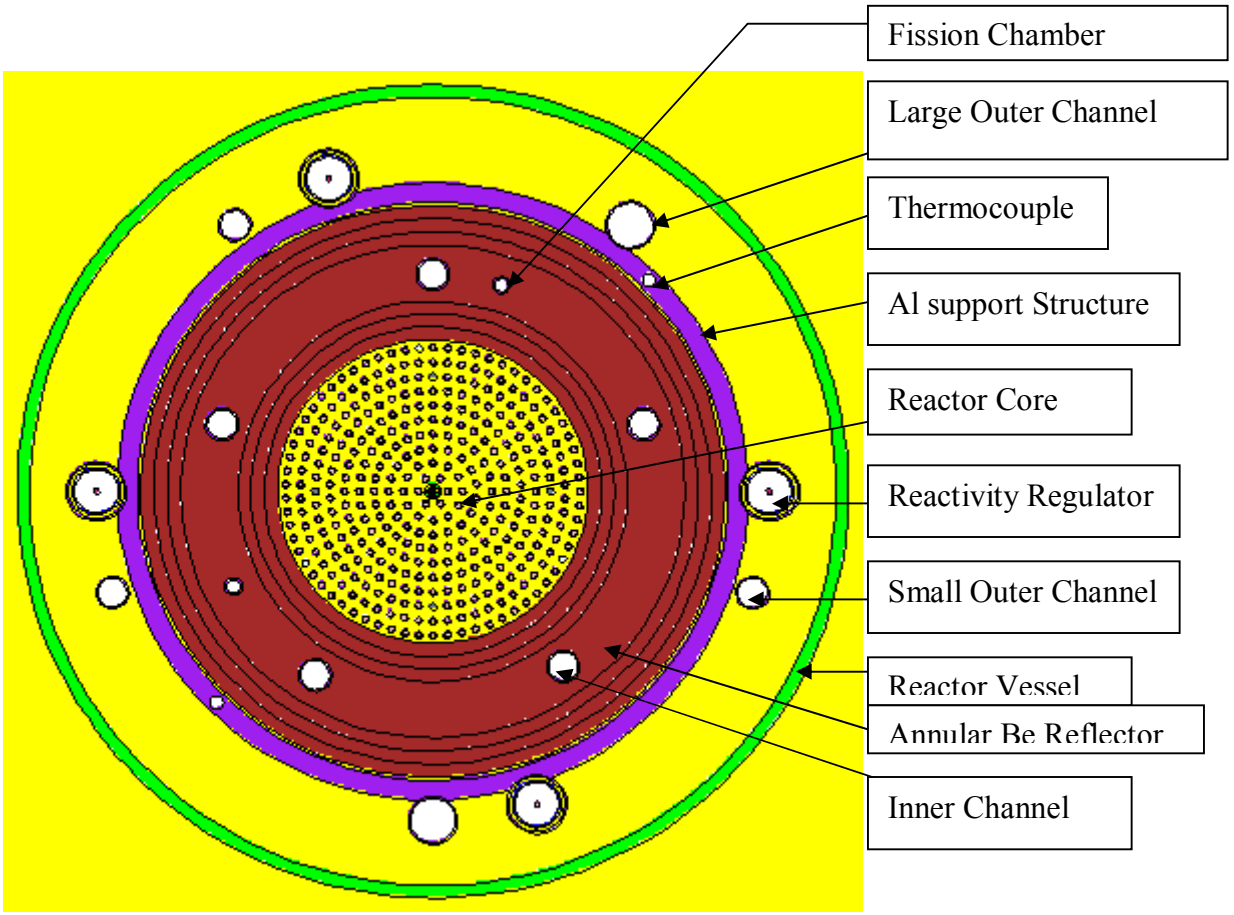


Fig.3.1. NIRR-1 Core configuration showing irradiation channels

3.1.5 Gamma ray spectrometer.

After the irradiation, the induced activities in the foils will be measured on a GEM-30195 HPGe coaxial, vertical dip-stick detector (ORTEC), which has a relative efficiency of 10% and resolution of 1.95keV, at 1.33MeV, ^{60}Co. The gamma-ray acquisition system consists of MAESTRO multi-channel Analyzer (MCA) emulation software card, coupled to the detector via electronic modules, all manufactured by ORTEC. The multi-purpose gamma ray analysis software, WINSPAN-2004 developed by Wang Liyu (2004) will be used for peak identification and evaluation

3.2 METHODOLOGY

3.2.1 Efficiency calibration of the HPGe

The standard gamma ray sources i.e. ^{22}Na, ^{54}Mn, ^{57}Co, ^{60}Co, ^{137}Cs, ^{152}Eu, ^{226}Ra and ^{241}Am were each placed on the sample holders, which were designed to be 1cm, 5cm and 15cm from the detector, and counted for 300s, 1800s and 4800s respectively. The net areas under the peaks, in the gamma ray spectrum, were recorded for each of the standards in the three source-detector geometries. The full energy peak (FEP) efficiency is then calculated and the efficiency versus energy response of the detector determined.

The full energy efficiency ε_p is calculated using the relation

$$\varepsilon_p = \frac{N_p / t_m}{A_t \ \gamma} x\, 100\% \qquad 3.1$$

where N_p = net area under the peak

t_m = measuring time

A_t = present activity, and

γ = gamma ray abundance.

The nuclear data used in the calculations is as shown in Table 3.1

In the semi-empirical method use was made of only four measured efficiency points. The model was built on the models developed by Gunnink, R. et al (1979) and (1988). This model views the 50keV to 4MeV calibration curve in three energy regions, i.e. $\leq$ 90KeV; 90-200KeV; and >200KeV.

50-90 keV region.

For large coaxial detectors, the efficiency is largely dependent on the active surface area of the detector and the attenuation in the detector end-cap (usually made of aluminum) and in the dead layer of the p-type germanium detectors. The source-to-detector distance is ignored since we are considering only the detectors intrinsic efficiency. The efficiency in this region is defined by

$$\varepsilon_E = \varepsilon^0 \exp(-\mu_{E.Al}.Al)\exp(-\mu_{E.Ge}.Ge) \qquad 3.2$$

where ε_E is the observed efficiency, ε^o is the ideal (no absorption) efficiency. $\mu_{E.Al}$ and $\mu_{E\,Ge}$ are the absorption coefficients (cm^2/g) for aluminum and germanium and Al, Ge are the thickness of aluminum and germanium, respectively (g/cm^2).

Since ε^o is the only unknown in equation 3.2, then we needed only one efficiency point i.e. the efficiency at 59.5 keV corresponding to ^{241}Am to completely characterize the efficiency curve in this region. The physical constants used in the calculations of efficiency in this region is as shown in Table 3.4

Table 3.4 Physical constants of Al and Ge used in the efficiency calculations.

Energy E(keV)	Mass attenuation coefficient (cm^2/g)	
	$\mu_{E.Al}$ x 10^{-3}	$\mu_{E.Ge}$ x 10^{-2}
20	68.330	33.769
30	18.445	10.869
40	7.235	4.821
50	3.506	2.547
60	1.954	1.447
70	1.365	1.060
80	0.777	0.626
90	0.578	0.475
100	0.379	0.324
ρ_{Al} =2.7 g/cm^3 ; ρ_{Ge} = 5.323 g/cm^3 Thickness of Al = 1.0 mm ; Thickness of Ge = 0.7mm		

*Data taken from Storm and Israel (1971)

>200kev region

The logarithm of efficiency above 200keV is nearly a linear function of the logarithm of energy. However, some distinct deviations from linearity must be accounted for in any accurate analytic description of the efficiency curve. Thus, the polynomial expression below defines the efficiency in this region.

$$\ln \varepsilon_E = \sum_{j=1}^{6} a_j (\ln E)^{j-1} \qquad 3.3$$

Where E is the energy, in MeV, and the higher-order coefficients, a_j, (where j=3, 4, 5 and 6) describe the non-linearity of the efficiency curve in this region. These higher-order (non-linear) terms are all correlated with the detector volume. Since a_1 and a_2 are the only

unknowns in the expansion of equation 3.3 then, we need to use only two widely spaced efficiency points i.e. at 661.6keV and 1332.5keV corresponding to ^{137}Cs and ^{60}Co to determine the entire efficiency curve from 200keV to 4MeV. The first two coefficients in equations 3.3, i.e. a_1 and a_2 are the intercept and slope of the graph of log ε versus log E of these two widely spaced efficiency points. Where ε is the measured efficiency and E is the energy of the gamma ray. The higher order coefficients are given by

$$a_3 = 0.539 - 0.01611V + 1.566 \times 10^{-4} V^2 - 5.01 \times 10^{-7} V^3 \quad 3.4$$

$$a_4 = -0.13595 + 1.239 \times 10^{-3} V - 6.088 \times 10^{-6} V^2 \quad 3.5$$

$$a_5 = -0.2239 + 6.3 \times 10^{-3} V - 5.895 \times 10^{-5} V^2 + 1.852 \times 10^{-7} V^3 \quad 3.6$$

$$a_6 = -0.04057 + 1.606 \times 10^{-3} V - 1.416 \times 10^{-5} V^2 - 4.292 \times 10^{-8} V^3 \quad 3.7$$

where V is the detector volume and was calculated from the length and diameter of the detector given by the manufacturers to be 3.34cm and 4.47cm respectively.

90-200keV region

The following equation describes the efficiency curve in this region.

$$\ln \varepsilon_E = A_1 + A_3 [4.816 \ln (E) + (\ln E)^2] \quad 3.8$$

Since the values of ε_E were determined for the two boundary points at 90 and 200keV, in the 50-90kev and the >200keV regions, then the values for A_1 and A_3 in equation 3.8 was easily evaluated and hence the efficiency for all energies in the region.

3.2.2 Site characterization.

Site characterization refers to the determination of the neutron spectrum parameters of the irradiation sites i.e. thermal-to-epithermal neutron flux ratio, *f*, epithermal neutron flux parameter, α, Westcott's $g(T_n)$ factor, Maxwellian neutron temperature, (T_n) and the

modified spectral index, $r(\alpha)\sqrt{T_n / T_0}$. In this work, an inner irradiation channel (A_1) and an outer irradiation channel (A_2) were selected as representatives of all the irradiation channels. For the determination of f and α values, the "Cd-ratio for multi-monitor" method was used because of its suitability for a priori f and α monitoring in reactors with stable neutron spectrum parameters such as MNSR and SLOWPOKE facilities. Based on four monitor reactions, detector foils were prepared from high-purity metals/alloys, which are recommended for neutron spectrum monitoring in reactor irradiation channels.

Two sets of detector foils were prepared for each of the irradiation channels. One set was arranged in a stack inside a vial for the 'bare' irradiation and the second set arranged in a stack inside 1 mm thick Cd-cover and kept inside the vial for the Cd-cover irradiation.

In channel A_1, the irradiations were carried out for 45 minutes for the 'bare' and 1¼ hours for the Cd-covered, while for channel A_2, the outer irradiation channel; the irradiation time was increased by a factor of 2 since the neutron flux in the outer channel is half the value in the inner channel. All irradiations were performed at a thermal power level of 15.5 kW, which corresponds to a preset neutron flux of 5.0×10^{11} n/cm^2 on the control console.

After the irradiation, the multi-purpose gamma ray analysis software WinSPAN-2004 was used for the peak identification and evaluation. For peak analysis of ^{69m}Zn and ^{198}Au nuclides, the irradiated foils were counted within a day after appropriate cooling time at a source-detector distance of 5cm to eliminate errors due to coincidence and pile-up losses. For peak analysis of ^{65}Zn and ^{95}Zr radionuclides, irradiated foils were counted at least one week after irradiation at a close source-detector distance of 1cm. The nuclear data

for the nuclides used is as shown in Table 3.5 and the irradiation, decay and counting regimes is given Tables 3.6a and 3.6b.

Table 3.5 Nuclear data for the nuclides used as monitors.

Monitor Reaction	$\overline{E}_r$, eV	Q_0	F_{Cd}	γ-Line measured, keV	Half-life
$^{197}Au(n,\gamma)\ ^{198}Au$	5.65	15.7	0.991	441.8	2.695 d
$^{68}Zn(n,\gamma)\ ^{69m}Zn$	590	3.19	1	438.6	13.76 h
$^{64}Zn(n,\gamma)\ ^{65}Zn$	2560	1.908	1	1115.5	244.3 d
$^{94}Zr(n,\gamma)\ ^{95}Zr$	6260	5.31	1	724 +756.7	64.02 d
$^{176}Lu(n,\gamma)\ ^{177}Lu$	0.158	-	-	112.9 & 208.4	6.73 d

Table 3.6a Irradiation, decay and counting regimes for irradiation site A1.

Irradiation site	**Isotope**	**Sample Wt (mg)**	**T_{-irr}(s)**	**T_d(s)**	**T_m(s)**
A1	**^{197}Au** (bare)	0.0139	2700	3600	1800
	Cd-covered	0.0132	4500	1500	1800
	^{68}Zn (bare)	0.0051	2700	2580	600
	Cd-covered	0.0049	4500	3840	1800
	^{197}Au (bare)	0.0139	2700	340140	300
	Cd-covered	0.0132	4500	344400	300
	^{175}Lu (bare)	0.0023	2700	338160	1800
	^{94} Zr (bare)	0.0448	2700	601080	2700
	Cd-covered	0.0452	4500	599040	5400
	^{64}Zn (bare)	0.0051	2700	609240	1200
	Cd-covered	0.0049	4500	608100	4500

Table 3.6b Irradiation, decay and counting regimes for irradiation site A2

Irradiation site	Isotope	Sample Wt (mg)	T_{-irr}(s)	T_d(s)	T_m(s)
A2	^{198}Au (bare)	0.0135	4500	6000	1200
	(covered)	0.0133	9000	1020	1800
	^{68}Zn (bare)	0.0049	4500	4860	900
	(covered)	0.005	9000	6540	1800
	^{198}Au (bare)	0.0135	4500	332340	300
	(covered)	0.0133	9000	332340	300
	^{175}Lu (bare)	0.0023	4500	328320	3600
	^{94}Zr (bare)	0.0446	4500	1728960	3600
	covered)	0.0447	9000	1716600	7200
	^{64}Zn (bare)	0.0049	4500	1732740	1000.18
	(covered)	0.005	9000	1724100	7200

a) Determination of *f*.

The "Cd-ratio for multi-monitor" method was used for the determination of flux ratio of thermal to epithermal neutrons, f. It involves irradiating bare and cadmium covered monitors and thereafter determining their induced activities. The parameter f is defined as

$$f = Q_{0,i}.(\alpha).(F_{Cd,i}.R_{Cd,r} - 1).\frac{G_{e,i}}{G_{th,i}} \qquad 3.9$$

where i is the monitor with well known Q_o-value, which is irradiated with and without Cd-cover. G_{th} and G_e are the correction factors for thermal and epithermal neutron self shielding, F_{cd} is the Cd-transmission factor for epithermal neutrons and the cadmium ratio

$$R_{Cd} = \frac{A_{sp.bare}}{A_{sp.Cd}}. \qquad 3.10$$

and $$A_{sp} = \left[\frac{N_p / t_m}{wSDC} \right] \qquad 3.11$$

where $A_{sp\ bare}$ and $A_{sp\ Cd}$ are the specific activities (specific count rates) of the bare and cadmium covered targets of ^{65}Zn, ^{95}Zr and ^{198}Au, N_p is the number of counts in the full energy peak, w is mass of monitor, t_{ur} = irradiation time, t_m = measuring time, λ =Decay constant

$S = (1 - e^{-\lambda t_{irr}})$, saturation factor

$D = e^{-\lambda t_d}$, Decay factor

$C = (1 - e^{-\lambda t_m})$, Counting factor

Thus, by calculating A_{sp} and R_{Cd} and substituting the values obtained in equation 3.9, the value of f, for the two irradiation sites A_1 and A_2, was determined by solving the equation using an iterative procedure based on MS-EXCEL spreadsheet.

b) Determination of α.

After irradiation and appropriate cooling time of the bare and Cd-covered monitors, the induced activities of the four monitors were measured with the HPGe detector whose detection efficiency curve has been determined. With all the monitors obeying the $\sigma(\nu)$ versus $1/\nu$ dependence, α is given by the slope of the straight line plot of

$$\log \frac{\overline{E}_{r,i}^{\alpha}}{(F_{Cd.} R_{Cd,i} - 1) Q_{0,i}(\alpha) G_{e,i} / G_{\text{th,i}}} \quad \text{versus} \quad \log \overline{E}_{r,i} \qquad 3.12$$

Also, by using an iterative procedure based on MS-EXCEL spreadsheet for a set of N monitors, equation (3.12) can be rewritten as equation (3.13) below and the α-value is found as the root of the equation.

$$\alpha + \frac{\sum_{i=1}^{N}\left[\left(\log\overline{E}_{r,i} - \frac{\sum_{i=1}^{N}\log\overline{E}_{r,i}}{N}\right)\left(\log\frac{E_{r,i}^{\alpha}}{(F_{Cd,i}R_{Cd,i}-1)Q_{0,i}(\alpha)G_{e,i}/G_{th,i}} - \frac{\sum_{i=1}^{N}\log\frac{E_{r,i}^{\alpha}}{(F_{Cd,i}R_{Cd,i}-1)Q_{0,i}(\alpha)G_{e,i}/G_{th,i}}}{N}\right)\right]}{\sum_{i=1}^{N}\left(\log\overline{E}_{r,i} - \frac{\sum_{i=1}^{N}\log\overline{E}_{r,i}}{N}\right)^{2}} = 0 \qquad 3.13$$

where

M = atomic mass of target nucleus; ϑ = Isotopic abundance of target nucleus

$Q_{o,i}$ = I_o/σ_o is the ratio of resonance integral to thermal neutron capture cross section at neutron velocity of 2200 m/s for the i^{th} monitor.

γ = gamma ray abundance of residual radionuclide.

ϕ_{th} = Sub-cadmium (thermal) neutron flux

i. = Denotes the i^{th} monitor, N, the number of monitors used

$E_{r,i}$ is the effective resonance energy of the i^{th} monitor

From the graph of equation 3.12 and the solution to equation 3.13, the values of α were determined for the two irradiation sites A_1 and A_2.

c) Determination of Neutron flux

Thermal, epithermal and fast neutron fluxes were determined using the monitor foils mentioned earlier and given in Table 3.1. the determination was done via the $^{27}Al(n, p)^{27}Mg$ and $^{197}Au(n, \gamma)^{198}Au$ reactions respectively. The thin foil technique was utilized, in which the measurements were made with minimum disturbance of the surrounding neutron environment.

i) Thermal flux

The technique used consisted of irradiating the thin foils in the irradiation channels A_1 and A_2 of the NIRR-1, then counting the radioactive species formed with the HPGe detector, after the appropriate cooling time. The detector had previously been calibrated for absolute photopeak counting efficiency. All photopeaks were considered in order to take advantage of higher efficiency and abundance of the low energy peaks and low mass attenuation coefficient of high energy peaks. The thermal neutron flux was then calculated from the relation

$$\Phi_{th} = \frac{N_p M}{N_A \vartheta I_\gamma \varepsilon_p \sigma_0 (1 + r(\alpha)\sqrt{T_n / T_0}\, .s_0(\alpha)} \qquad 3.14$$

The results of these measurements are found in Table 4.9.

ii) Epithermal flux

The epithermal flux was measured via the same procedure as the thermal flux, but 1mm cadmium covers were used to shield the thermal neutrons. The epithermal flux was then determined from the relation

$$\Phi_{epi} = \Phi_{th} \,.\, r(\alpha)\sqrt{T_n / T_0} \qquad 3.15$$

where Φ_{th} is as given by Eq. 3.14. The results are as given in table 4.9.

iii) Fast flux

The same procedure was employed as in the determination of epithermal neutron flux, but the calculation was done using the relation

$$\Phi_f = \frac{N_p M \lambda}{0.6\sigma_0 \rho \theta w I_\gamma \varepsilon_p (1 - e^{-\lambda t_m})(e^{-\lambda t_i})(1 - e^{-\lambda t_c})} \qquad 3.16$$

The results are as found in Table 4.9.

d) Determination of Modified Spectral Index (MSI).

^{176}Lu (n, γ) ^{177}Lu is amongst the most serious cases of "non-1/v" reactions i.e. ($g(T_n \neq 1)$. A Lu foil and a 1/v ($g(T_n = 1)$ monitor (^{197}Au) were co-irradiated without Cd-cover in the irradiation sites A_1 and A_2 and counted after the appropriate cooling time. The Modified spectral Index (MSI), which is a measure for the epithermal to total neutron density ratio, was obtained from the Cd-ratio method using equation 3.17 below.

$$r(\alpha)\sqrt{T_n / T_0} = \frac{G_{th}.g(T_n)}{R_{Cd}F_{Cd}\left[\frac{g(T_n)(1eV)^{\alpha}}{K(1+2\alpha)E_{Cd}{}^{\alpha}} - \frac{2}{\sqrt{\pi}}W'(\alpha) + G_r.s_0(\alpha)\right] - G_r.s_0(\alpha)} \qquad 3.17$$

The solution to the above equation was obtained by using an iterative procedure based on MS-EXCEL spreadsheet. The $k_{0,Au}$ factors and related nuclear data used in the determination are given in Table 3.7 below. However, it should also be noted that the conversion of s_0 to $s_0(\alpha)$ and W' to W'(α) was performed using equations 3.18a and 3.18b.

$$s_0(\alpha) = s_0(\bar{E}_r)^{-\alpha}(1\ eV)^{\alpha} \qquad 3.18a$$

$$W'(\varepsilon) = W'(\bar{E}_r)^{-\alpha}(1\ \text{eV})^{\alpha} \qquad 3.18b$$

Table 3.7 $k_{0,Au}$ factors and related nuclear data .

Target	Formed nuclide	E_γ, keV	k_0	Iγ	M	θ	s_0	E_r	G_e	G_{th}	Φ_o
^{176}Lu	^{177}Lu	113	0.0416	6.4	174.967	0.0259	1.669	0.158	1	1	2.1E-21
		208	0.0714	11.0	174.967	0.0259	1.669	0.158	1	1	2.1E-21
^{197}Au	^{198}Au	411	1	95.56	196.97	1.0	17.24	5.65	1	1	9.87E-23

e) Determination of Wescott's gT_n- factor and neutron temperature T_n

With the knowledge of the Modified Spectral Index, MSI, from above, the Maxwellian neutron temperature was determined using the equation 3.19 below.

$$g_{Lu}(T_n) = \left[\frac{A_{sp,Lu}/G_{th,Lu}}{\dfrac{k_{0,Au}(Lu)\varepsilon_{p,Lu}}{\dfrac{A_{sp,Au}}{k_{0,Au}(Au)\varepsilon_{p,Au}}}} \right] \left[G_{th,Au}.g_{Au}(T_n) + G_{r,Au}.r(\alpha)\sqrt{T_n/T_0}\,.s_{0,Au}(\alpha) \right] - G_{r,Lu}.r(\alpha)\sqrt{T_n/T_0}\,.s_{0,Lu}(\alpha)/G_{th,Lu} \quad 3.19$$

The solution to the above equation, which gives $g_{Lu}(T_n)$, was also obtained by using an iterative procedure based on MS-EXCEL spreadsheet. From the tables of $g_{Lu}(T_n)$ versus T_n, the value of the neutron temperature T_n, was finally obtained. The $g_{Lu}(T_n)$ versus T_n table is as shown in Table 3.8 below.

Table 3.8 $g_{Lu}(T_n)$ versus T_n

T_n	$g_{Lu}(T_n)$ Holden	$g_{Lu}(T_n)$ Grintakis & Kim
20 degree	1.7458	1.6914
40 degree	1.8922	1.8270
60 degree	2.0421	1.9651
80 degree	2.1932	2.1040

3.2.3 Cross sections and $k_{0,Au}$ determination.

Samples of the nuclides given in section 3.13, some of which were in powdered form, were each weighed and mixed thoroughly with aluminum oxide in such a ratio that the percentage of the nuclides in each sample ranged between 1 - 4 %. The aluminum helped in reducing the neutron self shielding effect in the samples. The samples, two of each, were then wrapped and heat-sealed in plastic bags. The polyethylene bags were

soaked in acid and cleaned with acetone to remove all traces of sodium which has a high thermal cross section. One set was arranged in a stack inside a vial for the 'bare' irradiation and the second set arranged in a stack inside 1 mm thick Cd-cover and kept inside the vial for the Cd-cover irradiation. The others, that are foils, were prepared in the same manner as the monitor foils described previously. From the measured activities of the samples after irradiation, the cadmium ratios were determined using eqn. 2.50. The cadmium ratios were then used to determine $Q_0(\alpha)$ values of the various nuclides using eqn. 2.72 followed by a conversion of $Q_0(\alpha)$ to Q_0 according to eqn. 2.68. The Q_0 values were then used to determine the activation cross sections using eqn. 2.37. Using the equation 3.20 the $k_{0,Au}$ were also determined.

$$\sigma_0 = k_{0,Au} \frac{\theta_{Au} \sigma_{0,Au} \gamma_{Au}}{M_{Au}} \cdot \frac{M}{\theta \gamma} \qquad 3.20$$

CHAPTER FOUR

RESULTS AND DISCUSSIONS

4.1 Calibration.

Standard gamma-ray emitting sources were used to determine the (FEP) efficiency of the HPGe detector. Three measured efficiency points were combined with the parameters of the detector to calculate the efficiency using semi-empirical method. The Figures 4.1a, 4.1b and 4.1c are the plots of the two widely spaced efficiency points for the determination of the first two coefficients in equations 3.3, i.e. a_1 and a_2. These coefficients are the intercept and slope of the graph of log , versus log E of these two points. A comparison of the measured/calculated efficiency as a function of gamma energy is as presented in figures 4.3a, 4.3b and 4.3c for the three different source-detector geometries.

In all three cases, the results show that the highest efficiency, for both measured and the semi empirical method is around 200keV. For close geometry, the measured efficiency is higher than the calculated efficiency by about 5% at the peak efficiency, while at 5cm source detector geometry the difference is higher (7%). In the farthest geometry, both measured and calculated efficiencies were a perfect fit. This may be attributed to the absence of random pile-up and coincidence summing up at large source to detector geometries. The results also show that the detection efficiency of the HPGe detector decrease with source to detector distance, i.e. the highest efficiency being at the closest geometry for a given gamma-ray energy. The detection efficiency curve of the HPGe detector has thus been determined for gamma energies higher than standard sources could provide, i.e. higher than 3 MeV.

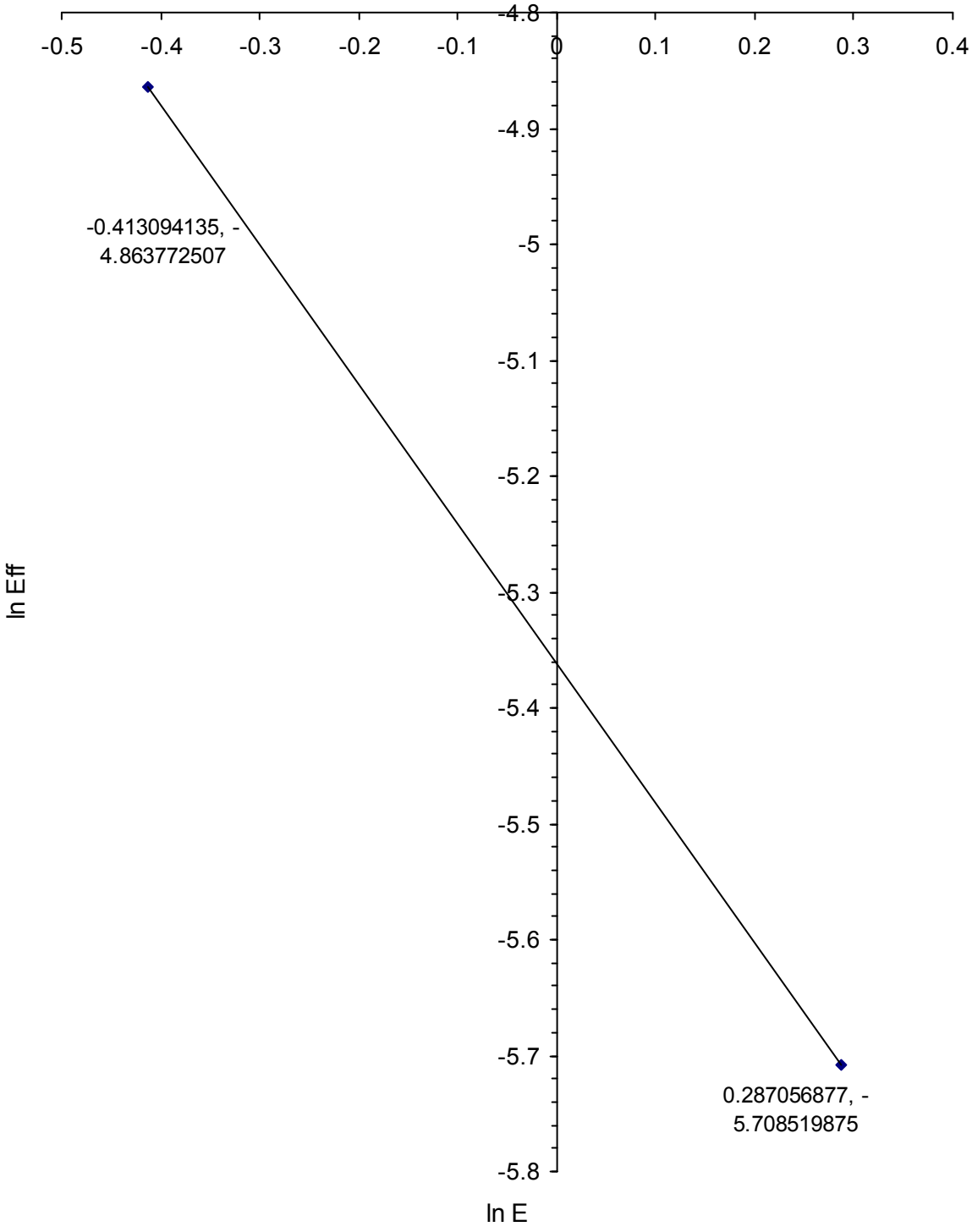


Fig.4.1a ln Eff. vs ln E at 1cm source-detector distance and energy range of 661.6 keV to 1332.5 keV

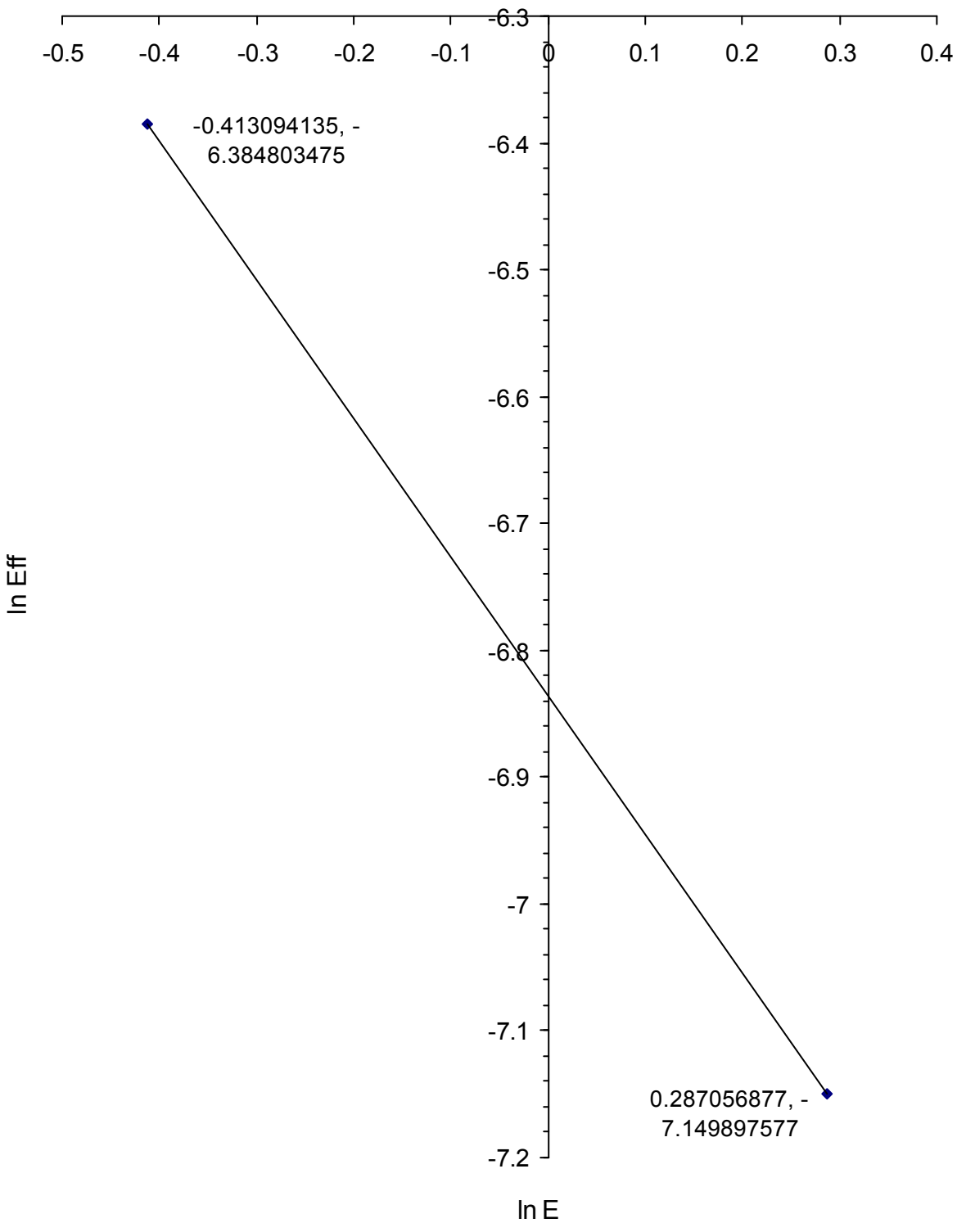


Fig.4.1b ln Eff. vs ln E at 5cm source-detector distance and energy range of 661.6 keV to 1332.5 keV

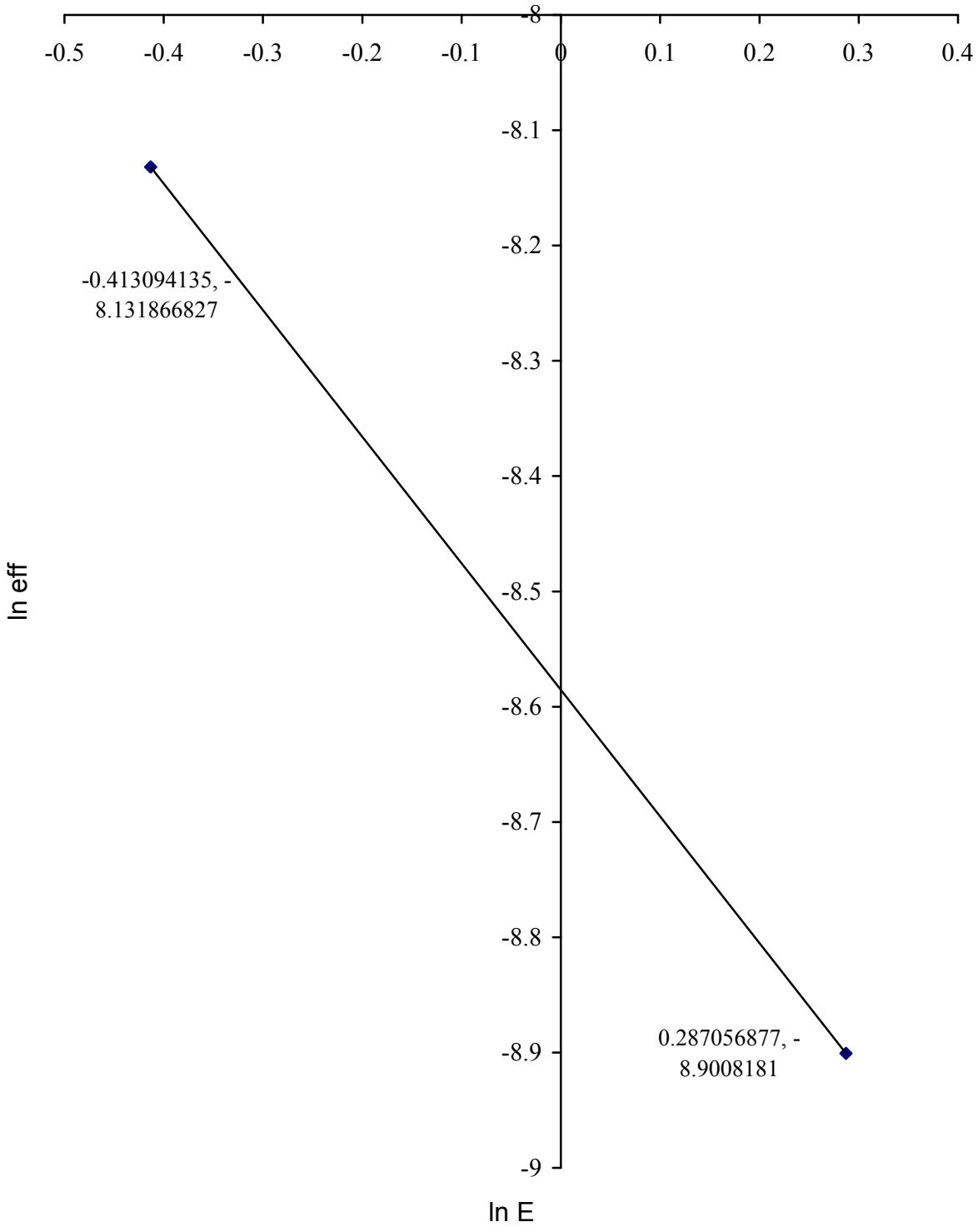


Fig.4.1c ln Eff. vs ln E at 15cm source-detector distance and energy range of 661.6 keV to 1332.5 keV

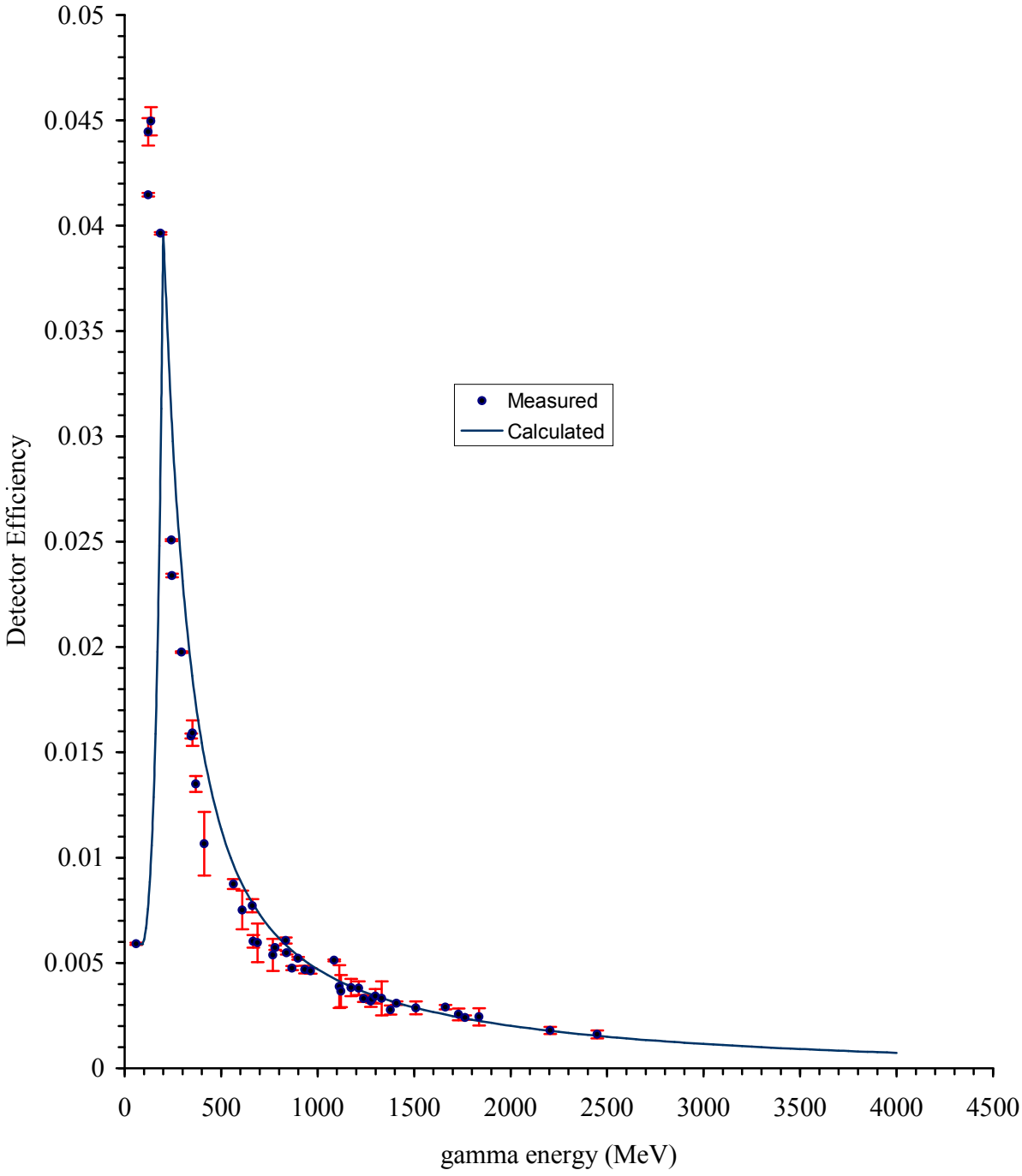


Fig.4.2a Measured/calculated efficiency of a HPGe detector vs gamma energy (close geometry)

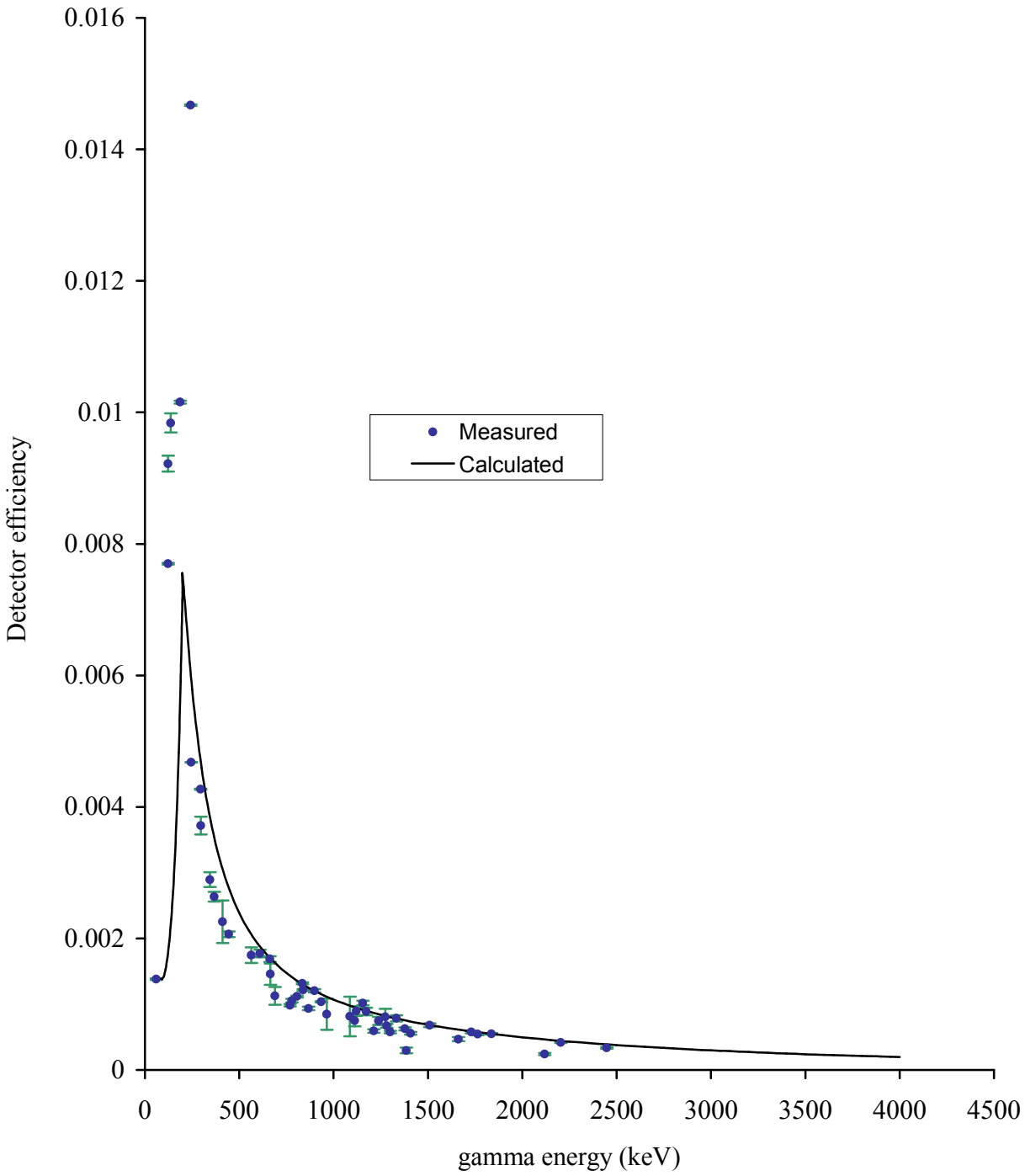


Fig.4.2b Measured / Calculated efficiency vs gamma energy for a HPGe detector (far geometry)

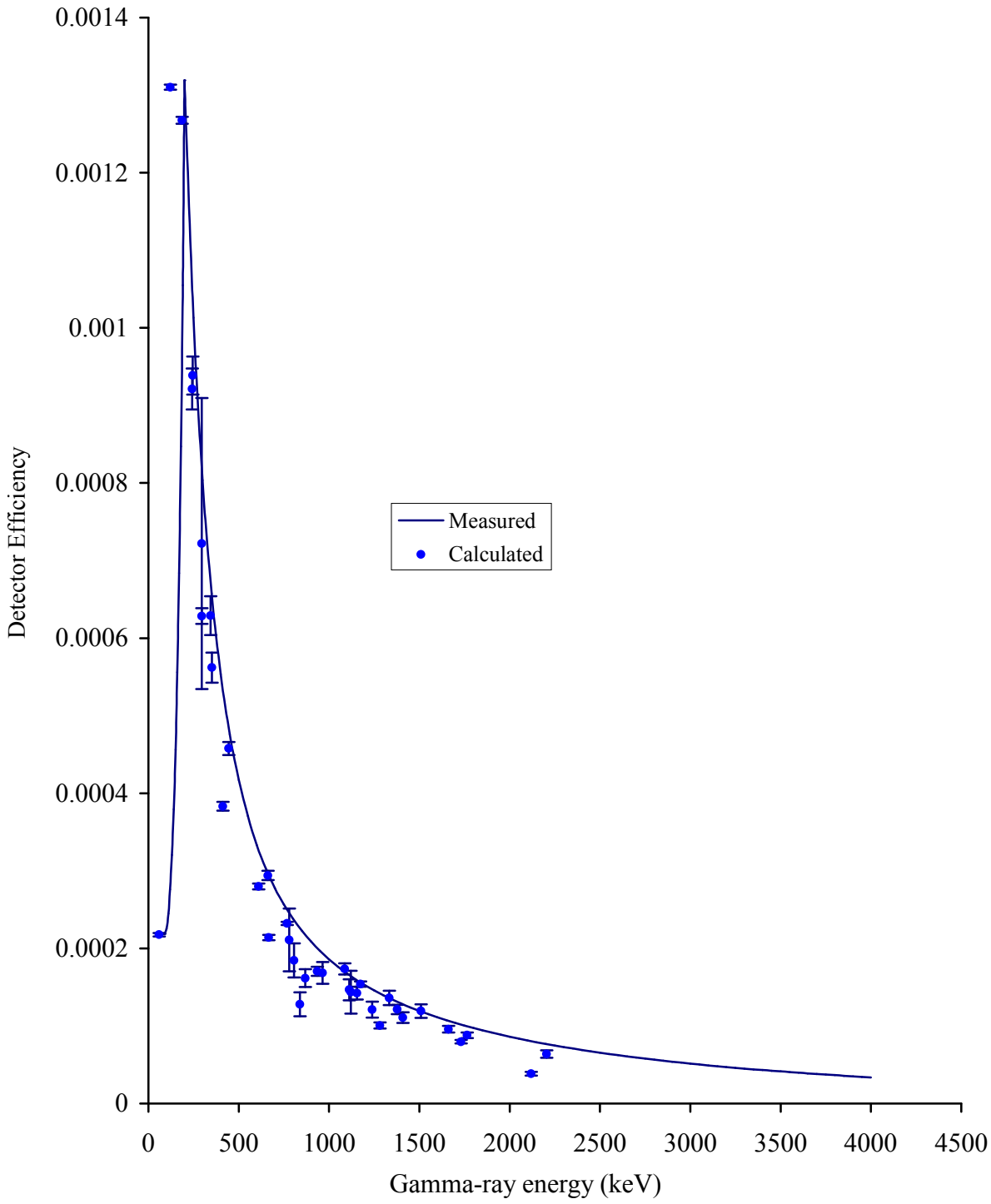


Fig.4.2c Measured/calculated efficiency vs gamma energy for HPGe detector at 15 cm

4.2 Cadmium ratios.

The measured cadmium ratios of the three flux monitors used in the determination of f and α were determined from the ratio of specific activity, A_{sp} of foil irradiated without to that irradiated with Cd-cover. The values are given alongside values obtained by Jonah, 2005 from other channels of NIRR-1 in Table 4.7 below.

Table 4.7 Calculated values of R_{Cd} for NIRR-1 and nuclear data of detector monitors**.**

Site	Target nucleus	Product nuclide	Half life	R_{cd}		Reference
				Inner	Outer	
channels B2 and B4	^{197}Au	^{198}Au	2.695d	2.12 ± 0.02	4.27 ± 0.06	Jonah S. A. et al, 2005
	^{68}Zn	^{69m}Zn	13.76h	5.63 ± 0.08	18.82 ± 0.70	
	^{94}Zr	^{95}Zr	244.0d	3.33 ± 0.16	12.65± 0.96	
	^{64}Zn	^{65}Zn	64.02d	8.15 ± 0.08	31.27 ± 0.68	
channels A1 and A2	^{197}Au	^{198}Au	2.695d	2.10 ± 0.01	4.32 ± 0.03	This work
	^{68}Zn	^{69m}Zn	13.76h	5.48 ± 0.06	18.64 ± 0.35	
	^{94}Zr	^{95}Zr	244.0d	3.38 ± 0.09	12.53 ± 0.518	
	^{64}Zn	^{65}Zn	64.02d	8.28 ± 0.29	30.97 ± 1.95	

From the results, the values we obtained show a good agreement with the values reported by Jonah et al, 2005 to within 2%. This further confirms the stability of the neutron flux of the NIRR-1 as indicated in literature.

4.3 *f* and *α*

The determination of *f* and *α* was performed by the "Cd-ratio for multi-monitor" –method. The values of *f* and *α* obtained from the solution to equation 3.13 and also from the plot of equation 3.12 are given alongside values obtained from similar reactors in table 4.8. The plots of equation 3.12 for the determination of *f* and *α* are as shown in Figures 4.3 and 4.4.

The results of *f* and *α* for this work along with those of other MNSR was as presented in Table 4.8. The results indicate that the inner channels of the MNS reactors are poorly thermalized (indicated by the negative α values) in comparison with the outer channels. This is to be expected because of the compact nature of the reactor core, designed with relatively low critical mass and low value of $H/^{235}U$ atoms in the fuel lattice (i.e., core under moderation). This makes shimming effective and avoids frequent reloading of fuel elements as well as obtains a reasonably high value of thermal neutron flux in the Beryllium annulus for NAA. The thermal to epithermal flux ratios in the two channels considered were found to be 18.4 and 49.5 respectively.

The measured α value, for the inner irradiation channel of NIRR-1, compares very well with the values for Slowpoke-2 reactors, but falls short by about 56% when compared with that of GHARR-1. The *f* and α values for the outer irradiation channel compare well with values of other of the MNSR and Slowpoke facilities presented in Table 4.8. This confirms the assertion that reactors with similar fuel have identical neutron spectra. The slight deviation of our α-value from the one reported by Jonah et. al., 2005 for NIRR-1 could be attributed to the channel location with respect to the core and effects of moderation, which could lead to slight differences in spectral indexes between irradiation

channels. This is one of the reasons De Corte, et al (1982) recommended that the epithermal flux-shaping factor be measured for each irradiation channel.

Table 4.8 Comparison of f and α values in irradiation channels of Slowpoke and MNSR facilities.

Facility	**Inner channel**		**Outer channel**		**Reference:**
	f	**α**	**f**	**α**	
MNSR, GHARR-1; Ghana 90% ^{235}U.	18.8	-0.104	49	-0.0261	Akaho et al, 2002
MNSR, Prototype, Beijing, China, 90% ^{235}U	19.8	-0.009	58.5	+0.023	Kennedy et al, 2003
Slowpoke-2,DUSR,Halifax Canada, 20% 235U (site #2)	18.8	-0.0425	57.1	-0.0098	Kennedy et al, 2003
Slowpoke-2,DUSR,Halifax Canada, 20% 235U (site #3)	18.9	-0.0422	57.1	-0.0098	Kennedy et al, 2003
Slowpoke-2,Ecole polytechnic Montreal, Canada, 20% ^{235}U	19.8	-0.052	55.4	-0.006	Kennedy et al, 2003
MNSR, NIRR-1; Zaria, Nigeria, 90% ^{235}U (sites **B2** & **B4**)	19.2	-0.052	48.3	+0.029	Jonah et al, 2005
MNSR, NIRR-1; Zaria, Nigeria, 90% ^{235}U (sites **A1** & **A2**)	18.4 ± 0.34	-0.046 ± 0.005	49.5 ± 0.96	+0.024 ±0.002	**This work**

The values obtained are in good agreement with values obtained from other irradiation channels of the reactor, which is an indication of the stability of the neutron flux and also the dependability of the efficiency calibration of the HPGe detector.

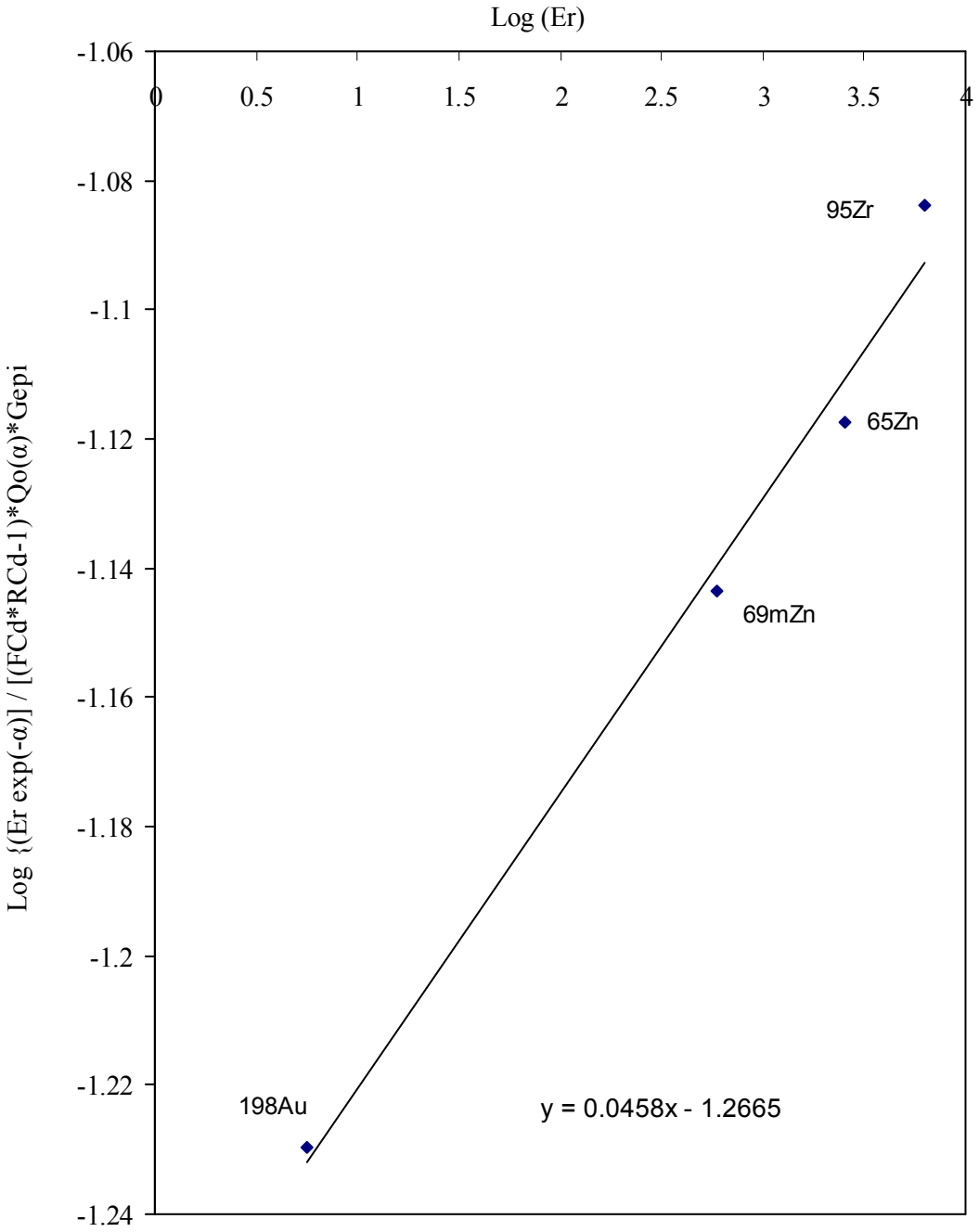


Fig.4.3 Plot for the determination of f and α by "Cd Ratio for multi monitor" method for an inner irradiation Channel A1, of NIRR-1

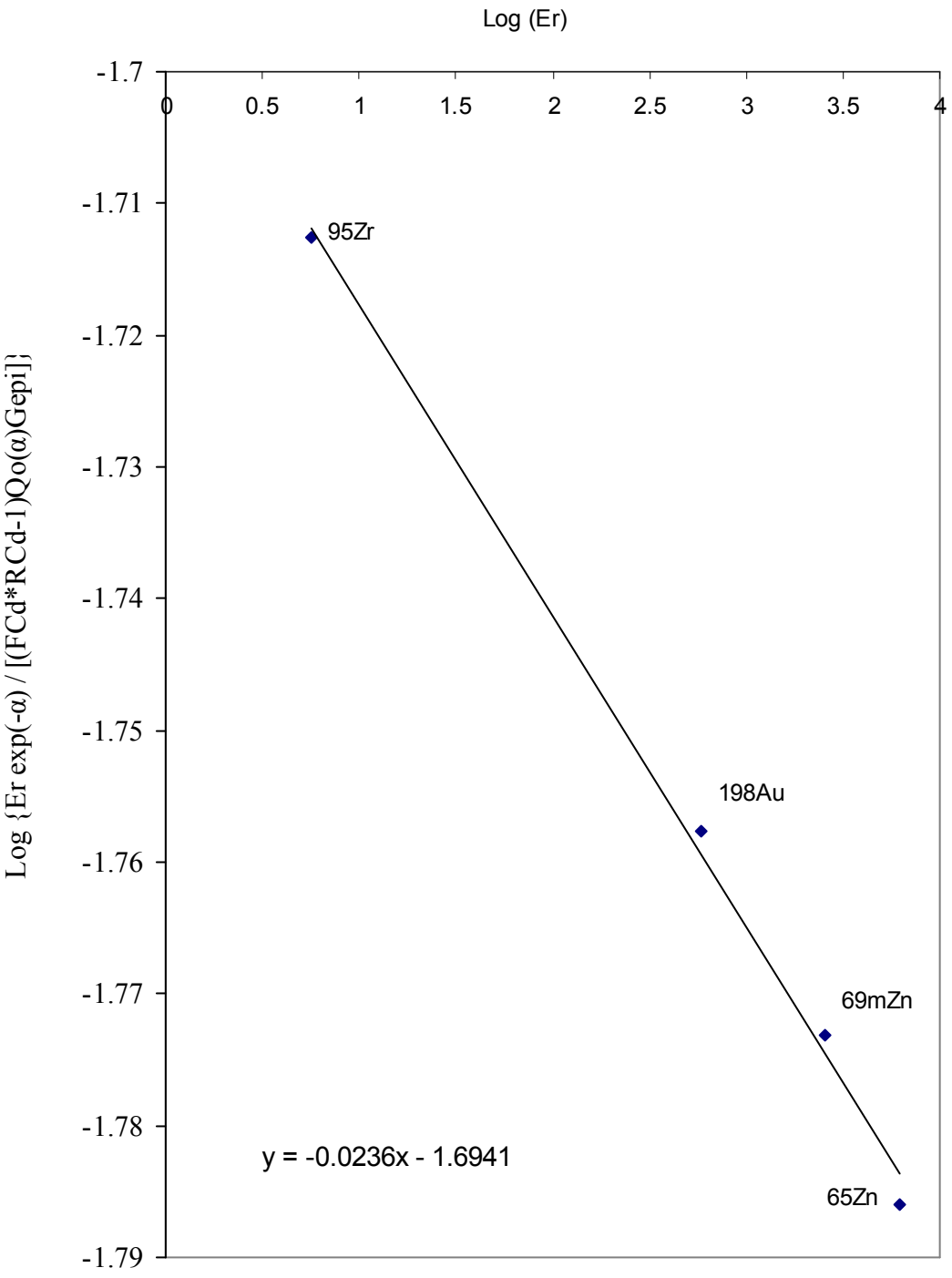


Fig. 4.4 Plot for the determination of f and alpha by "Cd Ratio multi monitor" method for an outer irradiation Channel, A2 of NIRR-1

4.4 Neutron flux

The average values of the flux measurements for the two irradiation sites A_1 and A_2 are as shown in table 4.9. The measurements were made using the Al-0.1%Au foil mentioned earlier and given in Table 3.1. The determinations for fast, epithermal and thermal flux were done via the ^{27}Al (n, p) ^{27}Mg, and ^{197}Au (n , γ) ^{198}Au reactions. It is apparent that the thermal neutron flux in A1 and A2 are very similar, but significantly lower in A2.

Table 4.9 Neutron fluxes.

Neutron Flux	Irradiation channel	
	Inner	**Outer**
Thermal	4.96×10^{11} n cm^2 s^{-1}	2.39×10^{11} n cm^2 s^{-1}
Epithermal	2.81×10^{10} n cm^2 s^{-1}	4.86×10^{9} n cm^2 s^{-1}
Fast	9.9×10^{11} n cm^2 s^{-1}	1.55×10^{10} n cm^2 s^{-1}

The results show that the inner irradiation site is poorly thermalized as compared to the outer irradiation channel and also confirms the assumption that the neutron flux in the inner channel is about twice that of the outer channel. The total neutron flux from the result also agrees with the neutron flux setting on the control console which was 5×10^{11} ncm^2 s^{-1}.

4.5 Westcott's g-factor, Modified Spectral Index and Neutron temperature.

The Westcott's g-factor is the ratio of the Maxwellian-averaged capture cross section to the 2200 ms^{-1} cross section. These factors, that account for the deviation from the ideal 1/E epithermal neutron flux distribution, approximated by a $\varphi'_e(E)$ α $1/E^{1+\alpha}$

behaviour with α independent of the neutron energy, were determined by co-irradiating Au and Lu foils and then determining their activities. The activities were then used to calculate these parameters using eqns. 3.17 and the results are shown in the Table 4.10.

Table 4.10. Westcott's g-factor, Modified Spectral Index and Neutron temperature.

Parameter	**Irradiation site**	
	Inner site A1	**Outer site A2**
$g(T_n)$	11.30	13.89
	1.883	1.821
$r(\alpha)\sqrt{T_n / T_0}$	0.04878	0.01786
$T_n T_n$	38.81^0 **(Holden)** 48.33^0 **(Gryntakis)**	30.22^0 **(Holden)** 39.05^0 **(Gryntakis)**

Results of T_n shows the temperature in the inner irradiation channel, A1, to be higher than that of the outer irradiation channel, A2, by approximately 9^0C. This may not be unconnected with the fact that the outer channel is positioned farther away from the core.

The value of the g-factor depends on whether the strongest resonance is at a positive or at negative neutron energy. When the strongest resonance is at positive neutron energy, the cross-section will be increasing as the energy approaches the resonance peak energy and the g-factor will be larger than unity. As the temperature increases, the Maxwellian distribution of neutron energies will further approach the peak cross-section value and the g-factor will increase with increasing temperature. Thus is the case with our result where the g-factor is greater than unity and increases as the temperature increases.

The modified spectral index, which is a measure for the epithermal to total neutron density ratio was found to be 0.04878 and 0.01786 for the inner A1 and outer A2 irradiation channels respectively.

4.6 Cross-sections.

For these determinations, the cadmium ratio was used. The nuclear data for the nuclides used and the cross section for gold, which is the universal comparator, were taken from De Corte, 2003. The resulting activation cross sections of 10 (n, γ) reactions obtained are compared to the evaluated values by Mughabghab, 2003, the SG-23 library, 2002, k_0/Nudat as well as other nuclear data libraries and is as presented in Table 4.11.

1. ^{197}Au (n, γ) ^{198}Au reaction.

   Though this is not among the reactions whose activation cross section is in doubt, but our result is in excellent agreement with the evaluated data from the nuclear data libraries, SG-23 and Mughabghab within a range of 0.1%.

2. ^{94}Zr (n, γ) ^{95}Zr reaction.

   Although the evaluated data from the libraries and Mughabghab agree with our results to within 13%, the values from the different libraries agree with each other to within almost the same margin.

3. ^{96}Zr (n, γ) ^{97}Zr reaction.

   Our result completely agrees with the results of the SG-23 but differ slightly with results from JENDL and Mughabghab to within 7%. The k0-Nudat value differs from JENDL and Mughabghab by about 14%.

4. ^{238}U (n, γ) ^{239}U reaction.

   Our results completely agree the evaluated data reported in the libraries and are also in excellent agreement with Mughabghab within a range of 2%

5. ^{55}Mn (n, γ) ^{56}Mn reaction.

The evaluated data reported by Mughabghab are in agreement with our results to within 0.4%. The results from JENDL also differ from Mughabghab by about the same margin.

6. ^{109}Ag (n, γ) ^{110m}Ag reaction.

The evaluated data reported by Mughabghab (2003) are in agreement with our results to within 10%., but differ significantly from results listed by JENDL.

7. ^{48}Ca (n, γ) ^{49}Ca reaction.

The evaluated data reported by Mughabghab and JENDL vary significantly with our results to within 22%. The results from IAEA-TECDOC, 1990 also differ from our results by about 26%.

8. ^{71}Ga (n, γ) ^{72}Ga reaction.

The evaluated data reported by Mughabghab and the other nuclear data libraries are in excellent agreement with our results to within 1.2%. Only the results from JENDL differ from our result by about 22%.

9. ^{74}Se (n, γ) ^{75}Se reaction.

The most significant difference from evaluated data reported by Mughabghab and the other nuclear data libraries is in this reaction, where the agreement with our results is to within 49%.

10. ^{75}As (n, γ) ^{76}As reaction.

The evaluated data reported by Mughabghab and JENDL are in excellent agreement with our results to within 3.5%. The results from SG-23 and k_0-Nudat differ from our result by about 7% and 14% respectively.

Table 4.11 Comparison of Calculated Activation cross section σ_0 and libraries.

Target	Product	Mughabghab	SG-23	k_0/Nudat	Jendl	This work
^{197}Au	^{198}Au	98.65 ± 0.09	-	-	-	98.74 ± 0.10
^{94}Zr	^{95}Zr	0.0499 ± 0.0024	0.04992	0.051	0.04981	0.043 ± 0.11
^{96}Zr	^{97}Zr	0.0229 ± 0.001	0.02118	0.0197	0.0228	0.021 ± 0.01
^{238}U	^{239}U	2.68 ± 0.019	2.75*	-	2.717	2.73 ± 0.03
^{55}Mn	^{56}Mn	13.36 ± 0.05	13.2*	-	13.41	13.31 ± 0.14
^{109}Ag	^{110m} Ag	4.7 ± 0.20	3.90*	-	90.53	4.24 ± 0.26
^{48}Ca	^{49}Ca	1.09 ± 0.07	1.12*	-	1.093	0.85 ± 0.24
^{71}Ga	^{72}Ga	4.73 ± 0.15	4.735(1.8)	4.650(0.8)	3.709	4.79 ± 0.005
^{74}Se	^{75}Se	51.8 ± 1.2	51.86(2.7)	50.50(4.8)	51.8	77.42 ± 9.14
^{75}As	^{76}As	4.23 ± 0.08	4.092(6.3)	3.85(4.8)	4.5	4.38 ± 0.03

A graphical comparison of our results with reported values from evaluated data libraries is also presented in Figure 4.5. The k_0-values for the various gamma energies of these 10 isotopes were also calculated and presented along with the other calculated parameters as shown in Table 4.12. The results also compares favorably with the evaluated values by Mughabghab and other compilations by De Corte et al, 2003. A graphical comparison of our values with Mughabghab is also given in Figure 4.6.

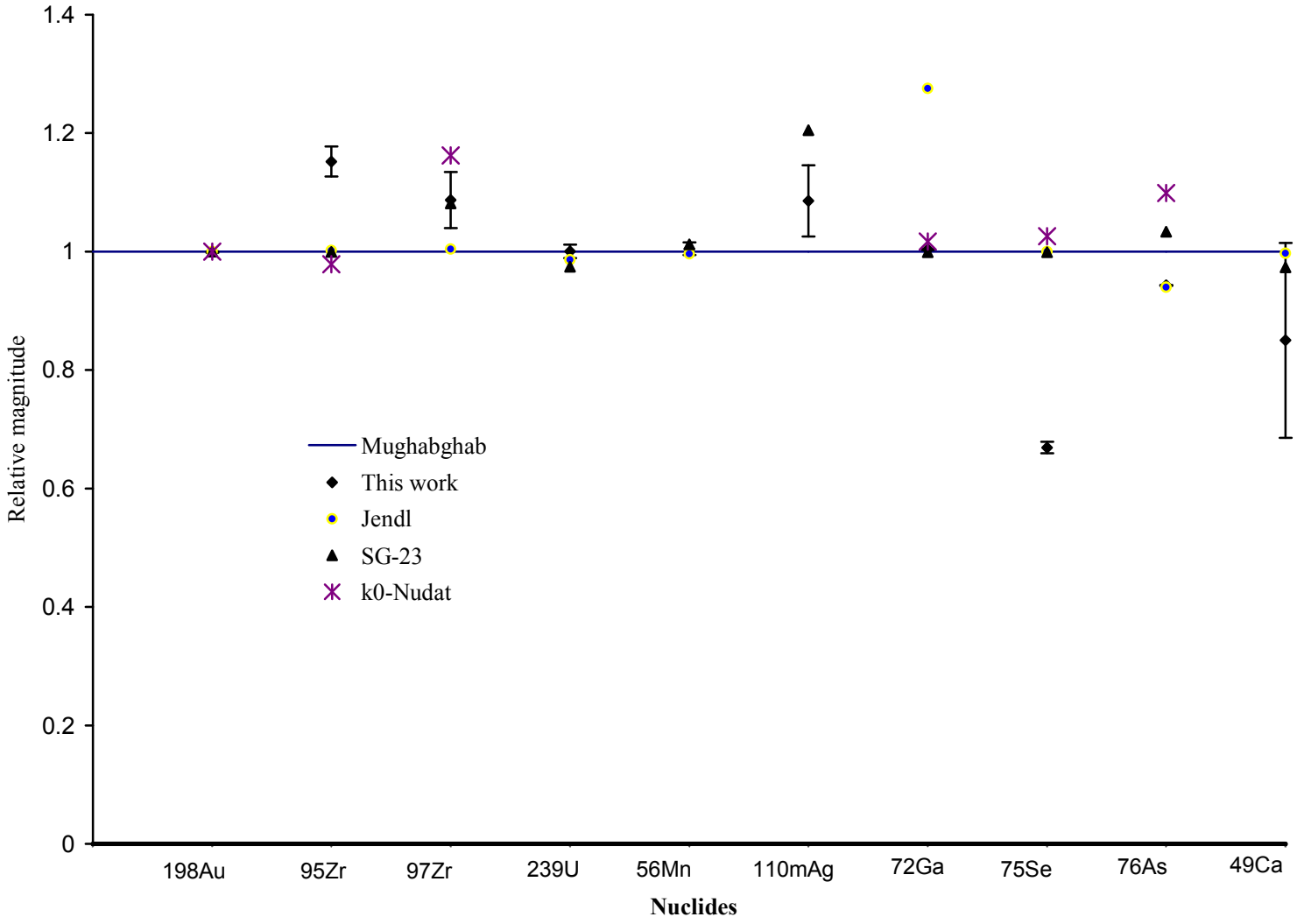


Fig.4.5Graphical comparison of Mughabghab with our result and other evaluated data

Table 4.12 Calculated k_0-factors and other parameters

Target	$Q_0(\alpha)$	Q_0	$I_o(\alpha)$	σ_o barns	Eγ	k_0
Au197	15.07227	15.697173	1.488E-21	98.726115	411.8	1
U238	95.092242	101.64325	2.591E-22	2.6789168	74.7	0.0118629
Mn54	0.9102804	1.0521942	1.211E-23	13.295347	846.8	0.5004865
					1810.7	0.1375074
					2113.1	0.0722925
Zr96	217.30428	249.26353	4.62E-24	0.0210652	254.2	1.706E-07
					355.4	3.089E-07
					507.6	6.849E-07
					602.4	1.88E-07
					703.8	1.276E-07
					1148.0	3.626E-07
Ga71	5.7897963	6.5194238	2.771E-23	4.7129909	630.0	0.0139325
					834.0	0.056885
					894.2	0.0056268
					1050.7	0.0039568
					2201.7	0.0148987
					2491.0	0.0042718
					2491.0 + 2507.8	0.0117315
					25.7.8 + 2515.7	0.0074608
Ag109	16.34073	17.050734	6.929E-23	4.3293413	446.8	0.0014526
					620.4	0.0010965
					657.8	0.0374471
					677.6	0.0042934
					687.0	0.0025652
					706.7	0.006729
					744.3	0.0018423
					763.9	0.0088381
					818.0	0.0028945
					884.7	0.0287988
					937.5	0.0135614
					1384.3	0.0096246
					1475.8	0.0015767
					1505.0	0.0051819
					1562.3	0.000468
Se74	6.2210469	6.72	4.8018E-22	77.4181	121.1	0.0030227
					136	0.0103189
					264.7	0.0107942
					279.5	0.0045553
					400.7	0.0020502
Zr94	4.3213969	5.3098864	1.872E-25	0.0433145	724.2	7.571E-05
					756.7	9.386E-05
					724.2 + 756.7	0.0001696
Ca48	0.8692295	1.2118103	6.384E-25	1.0853659	3084.4	9.693E-05
As75	12.484381	13.934474	5.465E-23	4.4852941	559.1	0.0543989
					559.1 + 563.2	0.0563504
					563.2	0.0019515
					657.1	0.0078061
					1212.9	0.0021955
					1212.9 + 1216.1	0.0067084
					1216.1	0.0045129

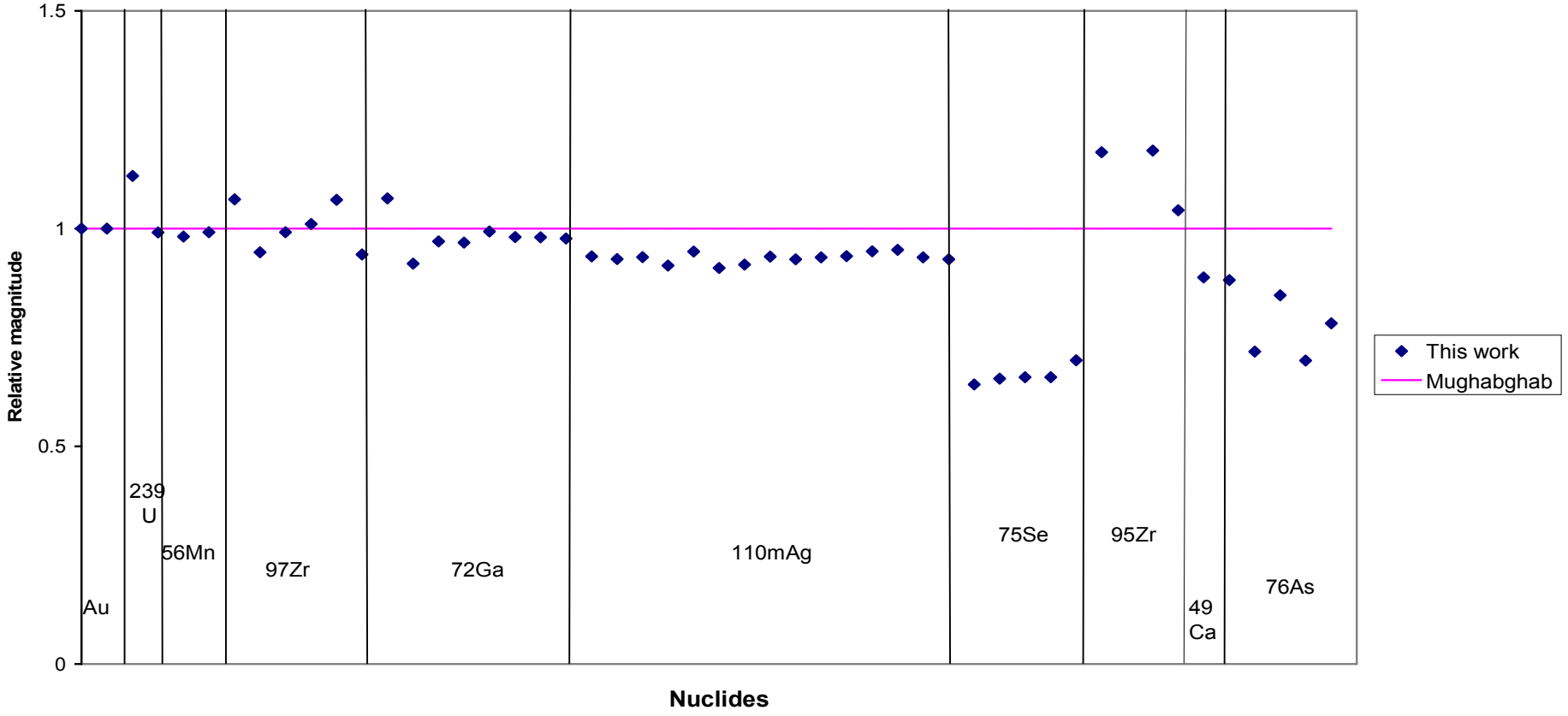


Fig. 4.6 A comparison of calculated k0-factors with Mughabghab

CHAPTER FIVE

CONCLUSION AND RECOMMENDATIONS

5.0 Conclusion.

For the purposes of characterizing the NIRR-1 and eventual determination of (n,γ) activation cross sections of ten capture reactions, the full-energy peak efficiency of the high purity germanium (HPGe) detector was measured with a good accuracy in the energy interval of 50-2500 keV for three different source-detector geometries. Further, using a semi-emperical method, three data points from the measured efficiency were used to calculate and extend the efficiency calibration up to 4000 keV for all the three source-detector geometries. From the results of the calibration, it is interesting to note that, the semi-empirical method gave a much higher efficiency at lower energies (~200keV), but evens out at higher energies for the 1cm and 5cm source-detector geometries. The 15cm source-detector geometry was an almost perfect fit for the measured and calculated efficiencies.

With the knowledge of the efficiencies of the HPGe detector, a complete characterization of the neutron flux spectra in the irradiation sites A1 and A2 of the NIRR-1 was also carried out and the results are in good agreement with previously reported values for irradiation sites B2 and B4 reported by Jonah et al, 2005. The Westcott's formalism was also employed to determine the values of the neutron temperature, T_n, modified spectral index, MSI and the Westcott's g-factor. These values i.e. f, α, T_n, MSI and g-factor agree with those reported from other MNSR's with similar configuration. It is worthy to note that, the negative α-value for irradiation site A1 corresponds to a "hardened' i.e. poorly thermalized irradiation channel due to the reactor core configuration and to the proximity of

the irradiation channel to the core. The thermal, epithermal and fast neutron fluxes were also determined independently using Al-0.1%Au foil via the ^{27}Al (n, p)^{27}Mg, and ^{197}Au (n, γ) ^{198}Au reactions and the total neutron flux was found to agree with the neutron flux registered on the control console. The thermal to epithermal flux ratio, f, in the two channels considered were found to be 18.4 and 49.5 respectively. Thus, with this result, the reactor (NIRR-1) can be said to have a completely characterized neutron spectrum parameters in four of its' six installed irradiation channels.

The knowledge of the neutron flux behaviour of the NIRR-1 enabled us to measure the Q_0- values and the subsequent determination of activation cross sections of 10 (n, γ) reactions. For this determination, the outer irradiation channel, A2 was used because it was discovered to be better thermalized than the inner irradiation channel, A1. With the reaction $^{197}Au(n, \gamma)^{198}Au$ as the standard, the results from seven of the nine reactions were found to be in excellent agreement to within 7% of those reported from evaluated data libraries. The results from the other two reactions i.e. $^{48}Ca(n, \gamma)$ ^{49}Ca and $^{74}Se(n, \gamma)$ ^{75}Se, were found to differ significantly (22% and 49%) from the evaluated data libraries. A further determination of the k_0-factors also showed the same degree of variations which indicates fairly good consistency.

5.1 Recommendations.

Since the main essence of this work is to verify and validate the evaluated data for those nuclides that are said to have discrepant data, therefore it would be proper to recommend the reevaluation of the Q_0, σ_0 and k_0 data for ^{49}Ca and ^{75}Se because of the wide discrepancy (22% and 49%) between our values and the evaluated nuclear data library.

REFERENCES

Acharya R.N., Nair A.G.C., Reddy A.V.R., and Manohar S.B., (2002). Validation of a neutron activation analysis method using k_0-standardization, *Journal of Applied Radiation and Isotopes. Vol. 57 pp391-398.*

Acharya, R. N., Chatt, A., (2003). Characterization of the Dalhousie University SLOWPOKE-2 reactor for k_0-NAA and application to medium-lived nuclides. *Journal of Radioanalytical Chemistry, vol. 257, pp525- 529*

Akaho, E.H.K., B.J.B. Nyarko., (2002). Characterization of neutron flux spectra in irradiation sites of MNSR reactor using Westcott-formalism for the k_0 neutron activation analysis method. *Journal of Applied Radiation and Isotopes. Vol. 57 pp265-273.*

Andrej, T., (2002). Validation of thermal cross sections and resonance integrals of SG-23 evaluated nuclear data library; *SG-23_ validation doc., IAEA.*

Breit, G., Weigner, E.P., (1936). *Physical Review, 49 pp519.*

De Corte F., Hammami, K. S., Moens, L., Simonits, A., De Wispelaere, A., Hoste, J., (1981). The accuracy of the experimental α-determination in the $1/(E^{1+\alpha})$ epithermal reactor neutron spectrum. *Journal of Radioanalytical Chemistry, vol. 62, pp209-255.*

De Corte F., Moens, L, Simonits, A., Hammami, K. S., De Wispelaere, A., Hoste, J., (1982). The effect of epithermal neutron flux distribution on the accuracy of absolute and comparator standardization methods in (n,γ) activation analysis. *Journal of Radioanalytical Chemistry, vol. 72, pp275-286.*

De Corte F., Simonits, A., De Wispelaere, A., Hoste, J., (1986). Compilation of k_0-factors and related nuclear data for 94 radionuclides of interest in NAA.*; INW/KFKI interim report(1986)*

De Corte, F., (1987) The k_0- Standardization Method -A Move to the Optimization of NAA; *Habiltation Thesis; University of Gent, Belgium*

De Corte F., Simonits, A., De Wispelaere, A., Hoste, J., (1987). Accuracy and applicability of k_0-standardization method, *Journal of Radioanalytical Chemistry, vol. 113, pp145-161.*

De Corte F., Simonits, A., Bellemans, F., Freitas, M.C., Javanovic, S., Smodis, B., Erdtman, G., Petri, H., De Wispelaere, A., (1993). Recent advances in k_0-standardization of neutron activation analysis; Extensions, applications,prospects; *Journal of Radioanalytical Chemistry, vol. 169, pp125-158.*

De Corte F., Bellemans, F., De Neve, P., Simonits, A., (1994). The use of modified Westcott-formalism in the k_0-standardization of NAA: The state of affairs; *Journal of Radioanalytical Chemistry, Article 179(1), pp 93.*

De Corte F.; Simonits, A. (2003). Recommended Nuclear Data for Use in the k_0-Standardization of Neutron Activation Analysis: *Atomic Data and Nuclear Data Tables 85, pp.47-67.*

De Wispelaere, A., De Corte, F., (2003). Recalibration of irradiation facilities in the Thetis reactor, with an examination of the α versus E behaviour in the keV neutron energy range*; Journal of Radioanalytical and Nuclear Chemistry, vol.257, pp.519-523.*

Doulers, Y., (1970). Thermal Neutrons. *IAEA Technical Reports on Neutron Fluence Measurements. Series No. 107. p 45-47.*

Evans R. D., (1982). The Atomic Nucleus. Krieger, New York

Frohner, F., (2000). JEFF Report 18. Evaluation and analysis of Nuclear Resonance Data

Glascock, M.D., (1996). Tables for Neutron Activation Analysis. The University of Missouri Research Reactor Center: Columbia, MO.

Gryntakis, E. M., Kim, J. I., (1975). Absorption, activation, and fission g(Tn) functions for non-1/v nuclides. *Journal of Radiochimica Acta 22; pp128-147.*

Gunnink, R., Niday, J.B., (1979). Proc. ERDA Symposium on X- and Gamma-Ray Sources and Applications, *Ann Arbor Science Publishers, Ann Arbor, Mich., p55.*

Gunnik, R., (1990): New method for calibrating a Ge detector by using only zero to four efficiency points; *Nuclear instruments and methods in physics research; A299, pp372-376.*

Høgdahl, O. T., (1962). Neutron absorption in pile neutron activation analysis; Michigan memorial phoenix project*, University of Michigan, Ann Arbor, Report MMPP-226.*

Holden, N. E., (1999). Temperature dependence on the Westcott g-factor for neutron reactions in activation analysis*.; Journal of pure applied chemistry, vol 71, No. 12, pp 2309-2315.*

Hoste J., (1988). Isotopic Neutron Source for Neutron Activation Analysis. *IAEA-TEC DOC-465.*

IAEA (1970). Neutron Fluence Measurements. Technical Report Series. No. 107. Vienna.

IAEA, (1990). Practical aspects of operating a neutron activation analysis Laboratory; *International Atomic Energy Agency IAEA-TEC DOC 564.*

Jonah, S.A., Balogun, G.I., Umar, I.M., Mayaki, M. C., (2005). Neutron spectrum parameters in irradiation channels of the Nigeria Research Reactor-1 (NIRR-1) for the k_0-NAA standardization. *Journal of Radioanalytical and Nuclear Chemistry, Vol. 266, No. 1, p 83-88.*

Jovanovich S., Vukotic P., Smodis B., Jacimovic R., Mihaljeric N., Stegnar P., (1989). Epithermal Neutron Flux Characterization of the Triger Mark II Reactor, Ljubljana, Yugoslavia for use in NAA. *Journal of Radioanalytical and Nuclear Chemistry, Vol. 129, No. 2, P343-349.*

Kennedy, G., St-Pierre, J., Wang, K.; Zang, Y., Preston, J., Grant, C., Vutchkov, M. (2000). Activation constants for SLOWPOKE and MNS reactors calculated from the neutron spectrum and k_0 and Q_0 values; *Journal of Radioanalytical and Nuclear Chemistry, Vol. 245, No. 1, pp167-172.*

Kim, J. I., Gryntakis, E. M., Born, H. J., (1975). Evaluation of the g(Tn)-function and determination of cross sections for Eu-isotope; *Journal of Radiochimica Acta 22; pp20-26.*

Knoll, F. G., (1979). Radiation Detection and Measurement. Cambridge University Press, New York.

Leo, R. W., (1987). Techniques for Nuclear and Particle Physics Experiment. A How to Approach. Springer Verley, Berlin Heidelberg, New York

Moens, L., De Corte F., De Wispelaere, A., Hoste, J., Simonits, A., Elek, A., Szabo, E., (1984). k_0 measurements and related nuclear data compilations for (n, γ) reactor neutron activation analysis part II*, Journal of Radioanalytical and Nuclear Chemistry, Articles 82/2, pp.385-452.*

Mossop G.M., (1968). Advanced Level Atomic Physics. University of London Press Ltd. pp.97.

Mughabghab, S. F., (2003): Thermal neutron capture cross sections, resonance integrals and g-factors; *International Atomic Energy Agency, INDC(NDS)-440.*

Rose, P. F. (Ed), (1991). ENDF/B-VI Summary Documentation*, BNL-NCS-17541 (ENDF-201), National Nuclear Data Center, Brookhaven National Laboratory*

Shibata, K., Kawano, T., Nakagawa, T., Iwamoto, O., Katakura, J. Fukahori, T., Chiba, S., Hasegawa, A., Murata, T., Matsunobu, H., Ohsawa, T., Nakajima, T., Yoshida, T., Zukeran, A., Kawai, M., Baba, M., Ishikawa, M., Asami, T., Watanabe, Y., Igashira, N., Yamamuro, N., Kitazawa, H., Yamano, N., Takano, H., (2002). Japanese Evaluated Nuclear Data Library Version 3- Revision 3: JENDL-3.3, *Nuclear Science and Technology. 39, 1125*

Singru, D., (1972). Introduction to Experimental Nuclear Physics. Wiley Eastern Private Limited, New York.

Simonits, A., De Corte, F., Hoste, J., (1975). Single comparator methods in reactor neutron activation analysis; *Journal of Radioanalytical and Nuclear Chemistry,24 pp.31-46.*

Simonits, A., Javanovic, S., De Corte, F., Moens, L., Hoste, J., (1984). A method for experimental determination of effective resonance energies related to (n, γ) reactions, *Journal of Radioanalytical and Nuclear Chemistry,vol.82, pp.169-174.*

Wang Liyu, 2004. *WINSPAN 2004*. A Multi Purpose Gamma-Ray Spectrum Analysis Software, CIAE, Beijing, China

Westcott, C. H.; (1960): Effective cross section values for well-moderated thermal reaction spectra; Atomic Energy of Canada ltd.; *TECH. Report CRRP-960, 3rd ed.*